

Chapter 2

Arrays and Spatial Filters

2.1 Introduction

We assume that we have a signal or multiple signals that are located in some region of a space-time field. We also have noise and/or interference that is located in some region of a space-time field. In the applications of interest these regions have some overlap.

An array is used to filter signals in a space-time field by exploiting their spatial characteristics. This filtering may be expressed in terms of a dependence upon angle or wavenumber. Viewed in the frequency domain this filtering is done by combining the outputs of the array sensors with complex gains that enhance or reject signals according to their spatial dependence. Usually, we want to spatially filter the field such that a signal from a particular angle, or set of angles, is enhanced by a constructive combination and noise from other angles is rejected by destructive interference.

The design of arrays to achieve certain performance criteria involves trade-offs among the array geometry, the number of sensors, signal-to-noise, and signal-to-interference ratios, as well as a number of other factors.

There are two aspects of array design that determine their performance as spatial filters. First, their geometry establishes basic constraints upon their operation. Line arrays can resolve only one angular component. This leads to a cone of uncertainty and right/left ambiguities. Circular arrays have different patterns than crossed or planar arrays. Frequently the geometry is established by physical constraints and the designer may have limited freedom in specifying the array geometry.

The second aspect is the design of the complex weightings of the data at each sensor output. The choice of these weightings determines the spatial

filtering characteristics of the array for a given geometry.

In this chapter we introduce the basic definitions and relationships that are used to analyze and synthesize arrays. Our approach is to introduce the concepts for an arbitrary array geometry. We then specialize the result to a uniform linear array and then further specialize the result to a uniform weighting. In Chapter 3, we return to linear arrays and provide a detailed discussion of the analysis and synthesis of linear arrays. In Chapter 4, we study the analysis and synthesis of planar and volume arrays.

This chapter is organized in the following manner. In Section 2.2, we introduce the frequency-wavenumber response function and beam pattern of an array. We employ wavenumber variables with dimensions of inverse length for a number of reasons. First, array coordinates and wavenumbers are conjugate Fourier variables, so Fourier transform operations are much simpler. Second, all the powerful properties of harmonic analysis as extended to homogenous processes can be used directly and the concept of an array as a spatial filter is most applicable. Third, angle variables specify array filter responses over a very restricted region of wavenumber space. While it does describe the response over the region for all real, propagating signals, that is, those space-time processes that implicitly satisfy a wave equation when one assigns a propagation speed and direction, there are a lot of advantages to considering the entire wavenumber space. The so-called virtual space, or wavenumber realm where real signals cannot propagate is very useful in the analysis of array performance.

In Section 2.3, we specialize these results to a uniform linear array and study the characteristics of the beam pattern. In Section 2.4, we further specialize these results to the case of a uniformly weighted linear array. This leads to a beam pattern that we refer to as the conventional beam pattern. It will play a fundamental role in many of our subsequent studies. In Section 2.5, we discuss array steering and show how it affects the beam pattern in wavenumber space and in angle space. In Section 2.6, we define three important performance measures:

- (i) Directivity
- (ii) Array gain
- (iii) Tolerance function

These performance measures are utilized throughout our discussion.

The discussion in the first six sections assumes that the sensors are isotropic (i.e., their response is independent of the direction of arrival of the signal). In Section 2.7, we introduce the concept of pattern multiplication to accommodate non-isotropic sensors. In Section 2.8, we consider the case

of a linear aperture and show how the performance of apertures and arrays are related. In Section 2.9, we give a brief summary of our development.

In Table 2.1, we have summarized the structure of the chapter. The various terms are defined at appropriate points in the chapter.¹

The material in this chapter can be termed **classical array theory**, and it has been discussed in a number of books and articles. References that we have utilized include Kraus [Kra88], Balanis [Bal82], Elliott [Ell81], Johnson [Joh93], Milligan [Mil85], Ziomek [Zio95], Skolnik [Sko80], Stutzman and Thiele [ST81], and Weeks [Wee68].

The coordinate system of interest is shown in Figure 2.1. The relationships between rectangular and spherical coordinates is shown in Figure 2.1.

$$\begin{aligned}x &= r \sin \theta \cos \phi, \\y &= r \sin \theta \sin \phi, \\z &= r \cos \theta.\end{aligned}\tag{2.1}$$

The next set of figures shows various arrays and apertures placed in this coordinate system.

Figure 2.2 shows a linear array with equally spaced elements. The polar angle θ is the grazing angle with respect to the positive z -axis. In some cases the broadside angle $\bar{\theta}$ is a useful parameter

$$\bar{\theta} = \frac{\pi}{2} - \theta.\tag{2.2}$$

The position of the elements is denoted by p_{z_n} ,

$$p_{z_n} = \left(n - \frac{N-1}{2} \right) d, \quad n = 0, 1, \dots, N-1,\tag{2.3}$$

where d is the interelement spacing.

Figure 2.3 shows a linear array with unequally spaced elements. In this case,

$$p_{z_n} = z_n,\tag{2.4}$$

where z_n is the z -coordinate of the n th element.

¹We have included a structure chart at the beginning of Chapters 2–9. Its primary purpose is to serve as a graphical *a posteriori* reference for the reader so that, after reading the chapter, one can easily find a particular topic. A secondary purpose is to aid an instructor in planning the coverage of the material.

Table 2.1 Structure of Chapter 2

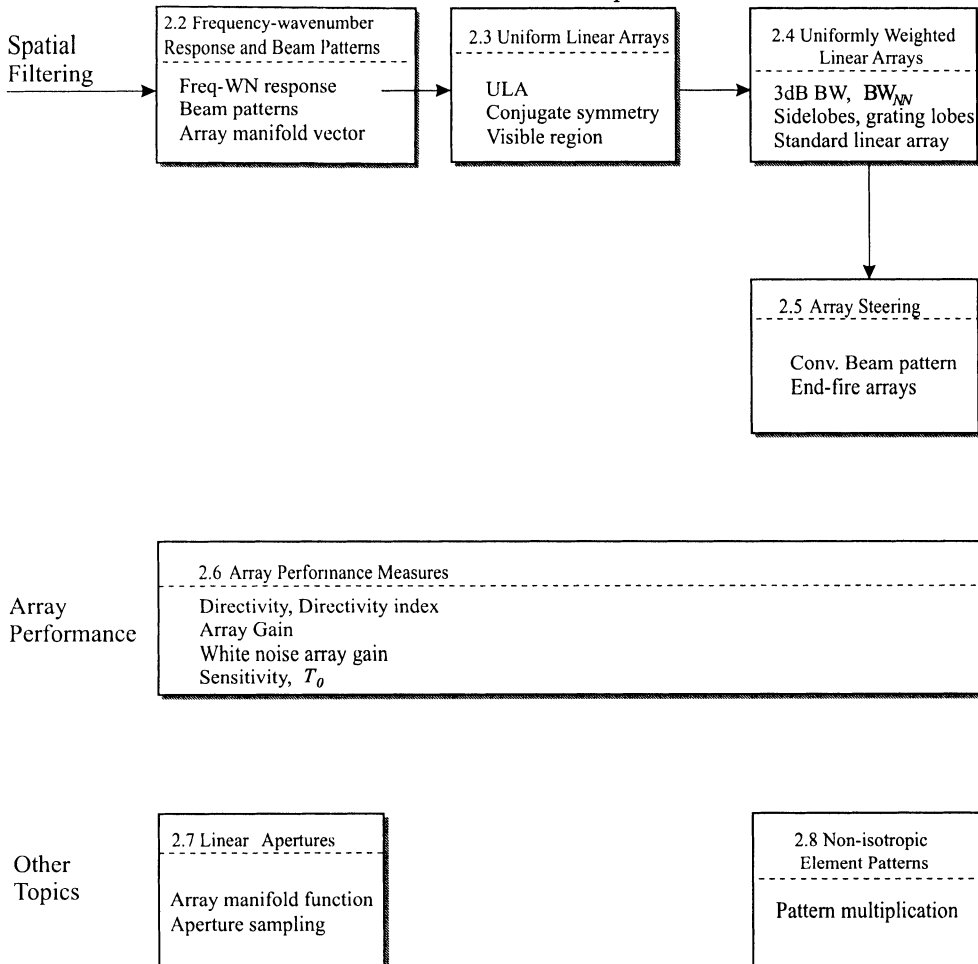


Figure 2.4 shows a continuous linear aperture along the z -axis. We would anticipate that if d is small and

$$L = Nd, \quad (2.5)$$

the array and aperture would have very similar performance. We demonstrate this relationship later. We also discuss how we sample a continuous aperture to obtain an array.

Figure 2.5 shows several examples of planar arrays that are of interest. Figure 2.6 shows the corresponding planar aperture. We define the coor-

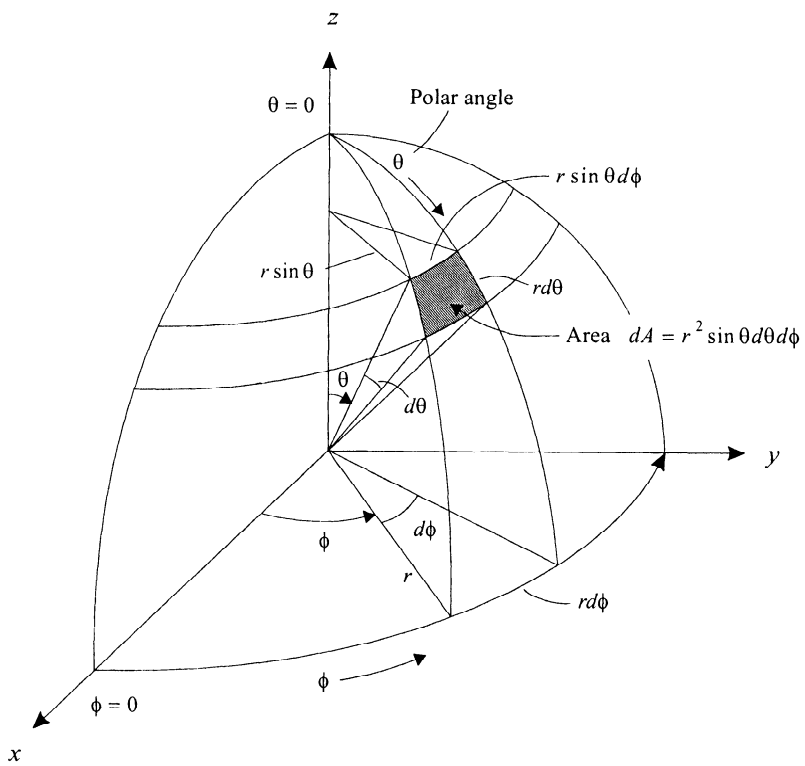


Figure 2.1 Spherical coordinate system.

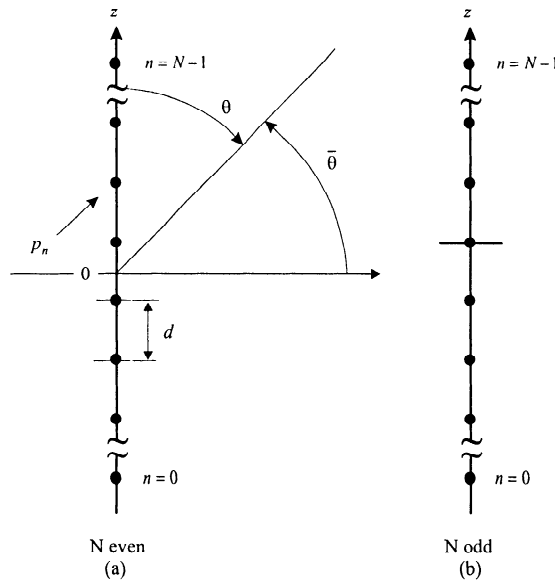


Figure 2.2 Linear array with equal spacing between elements: (a) N even; (b) N odd.

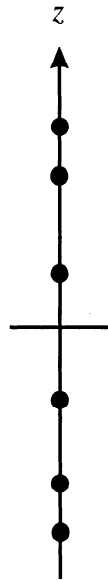


Figure 2.3 Linear array with unequal spacing between elements.

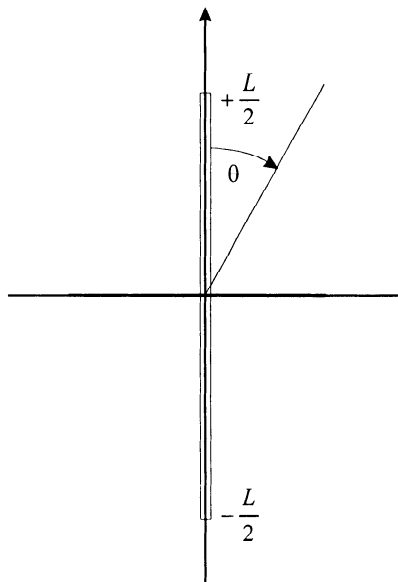


Figure 2.4 Linear aperture.

dinate system in detail in Chapter 4 where we analyze planar arrays and apertures.

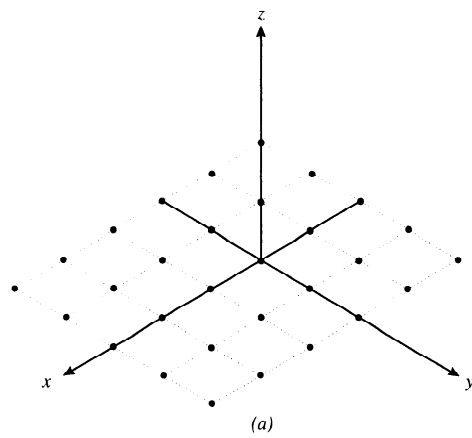
Figure 2.7 shows some volume arrays of interest. We will discuss volume arrays and apertures in Chapter 4.

2.2 Frequency-wavenumber Response and Beam Patterns

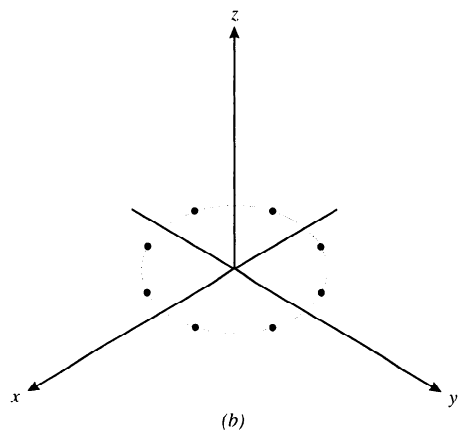
In this section, we analyze the response of an array to an external signal field. The array consists of a set of isotropic sensors located at positions \mathbf{p}_n , as shown in Figure 2.8. The sensors spatially sample the signal field at the locations $\mathbf{p}_n : n = 0, 1, \dots, N - 1$. This yields a set of signals that we denote by the vector $\mathbf{f}(t, \mathbf{p})$

$$\mathbf{f}(t, \mathbf{p}) = \begin{bmatrix} f(t, \mathbf{p}_0) \\ f(t, \mathbf{p}_1) \\ \vdots \\ f(t, \mathbf{p}_{N-1}) \end{bmatrix}. \quad (2.6)$$

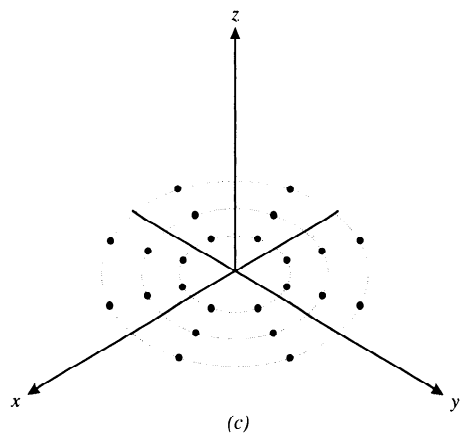
We process each sensor output by a linear, time-invariant filter with



(a)



(b)



(c)

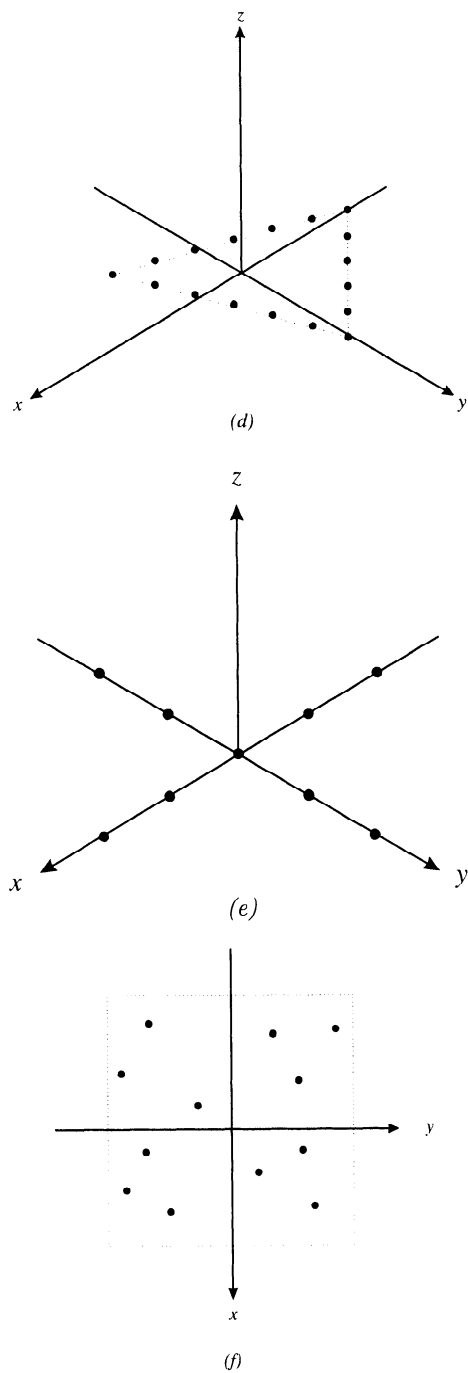


Figure 2.5 Planar arrays.

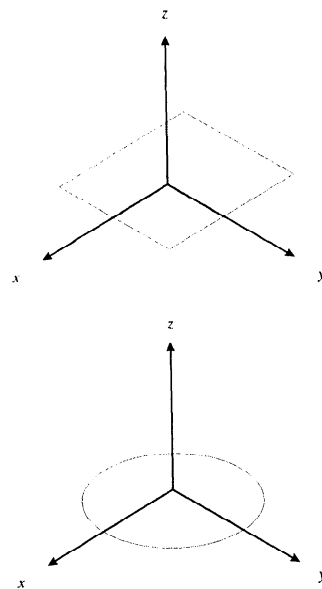


Figure 2.6 Planar apertures.

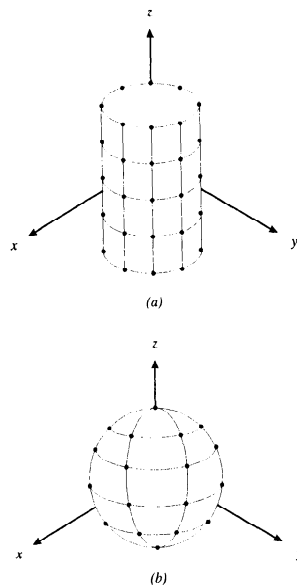


Figure 2.7 (a) Cylindrical array of identical, regularly spaced, omnidirectional point elements; (b) spherical array of identical, regularly spaced, omnidirectional point elements.

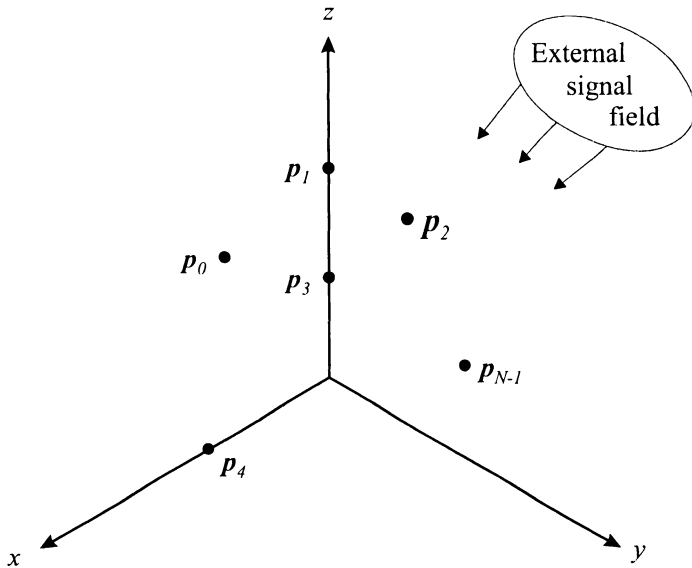


Figure 2.8 \$N\$-Element array.

impulse response $h_n(\tau)$ and sum the outputs to obtain the array output $y(t)$. The procedure is shown in Figure 2.9. We assume that the observation interval is long enough that it may be considered infinite. The output $y(t)$ can be written as a convolution integral,

$$y(t) = \sum_{n=0}^{N-1} \int_{-\infty}^{\infty} h_n(t - \tau) f_n(\tau, \mathbf{p}_n) d\tau. \quad (2.7)$$

This result can be written in vector notation as

$$y(t) = \int_{-\infty}^{\infty} \mathbf{h}^T(t - \tau) \mathbf{f}(\tau, \mathbf{p}) d\tau, \quad (2.8)$$

where

$$\mathbf{h}(\tau) = \begin{bmatrix} h_0(\tau) \\ h_1(\tau) \\ \vdots \\ h_{N-1}(\tau) \end{bmatrix}. \quad (2.9)$$

The result in (2.8) is a straightforward extension of familiar scalar results to the vector model.

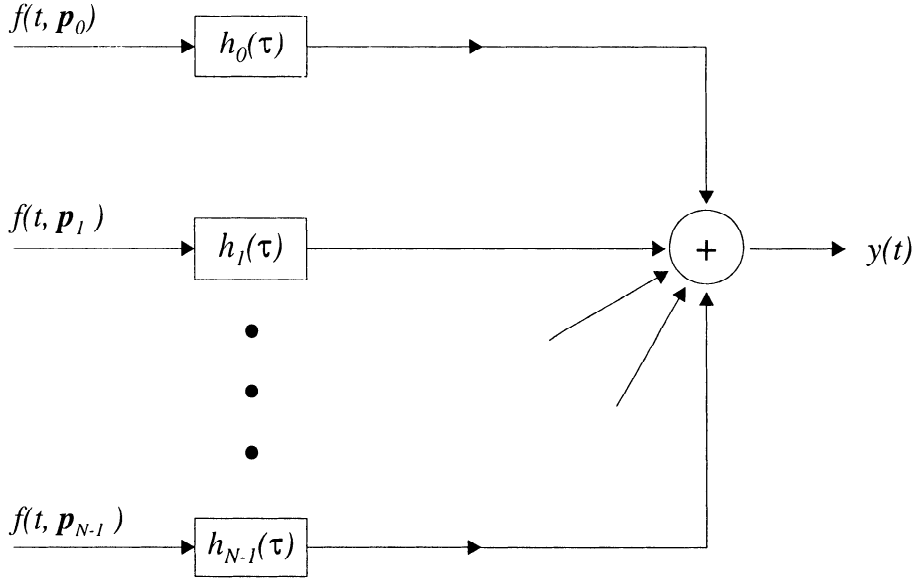


Figure 2.9 Array with linear processing.

Alternatively, we can write (2.8) in the transform domain as

$$\begin{aligned} Y(\omega) &= \int_{-\infty}^{\infty} y(t)e^{-j\omega t}dt \\ &= \mathbf{H}^T(\omega)\mathbf{F}(\omega), \end{aligned} \quad (2.10)$$

where

$$\mathbf{H}(\omega) = \int_{-\infty}^{\infty} \mathbf{h}(t)e^{-j\omega t}dt, \quad (2.11)$$

and

$$\mathbf{F}(\omega, \mathbf{p}) = \int_{-\infty}^{\infty} \mathbf{f}(t, \mathbf{p})e^{-j\omega t}dt. \quad (2.12)$$

In most cases, we suppress the \mathbf{p} dependence on the left side of (2.12) and use $\mathbf{F}(\omega)$.

To illustrate a simple beamforming operation, consider the case shown in Figure 2.10. The input is a plane wave propagating in the direction \mathbf{a} with temporal (radian) frequency ω . The time functions at the sensors due to this input can be written in two equivalent ways. The first way emphasizes the time delays corresponding to the time of arrival at the various sensors. If $f(t)$ is the signal that would be received at the origin of the coordinate

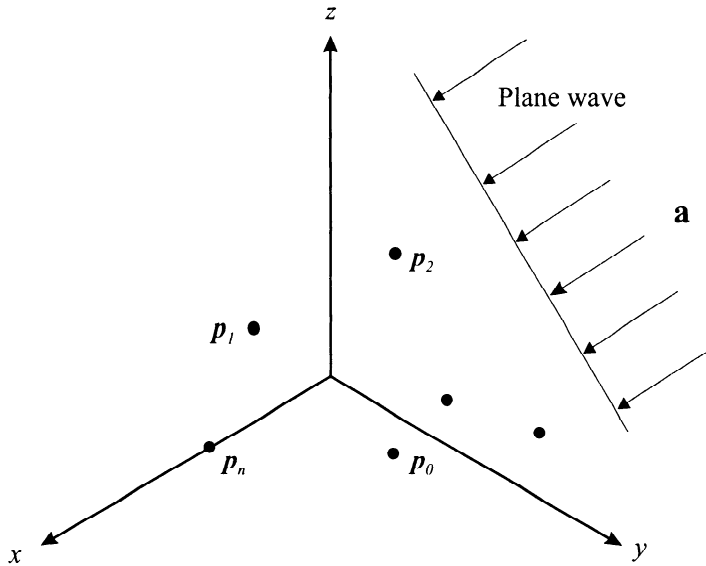


Figure 2.10 Array with plane-wave input.

system, then

$$\mathbf{f}(t, \mathbf{p}) = \begin{bmatrix} f(t - \tau_0) \\ f(t - \tau_1) \\ \vdots \\ f(t - \tau_{N-1}) \end{bmatrix}, \quad (2.13)$$

where

$$\tau_n = \frac{\mathbf{a}^T \mathbf{p}_n}{c}, \quad (2.14)$$

and c is the velocity of propagation in the medium and \mathbf{a} is a unit vector that can be expressed as

$$\mathbf{a} = \begin{bmatrix} -\sin \theta \cos \phi \\ -\sin \theta \sin \phi \\ -\cos \theta \end{bmatrix}. \quad (2.15)$$

The minus sign arises because of the direction of \mathbf{a} . Then, τ_n is given by

$$\tau_n = -\frac{1}{c} [\sin \theta \cos \phi \cdot p_{x_n} + \sin \theta \sin \phi \cdot p_{y_n} + \cos \theta \cdot p_{z_n}]. \quad (2.16)$$

If we define direction cosines with respect to each axis as

$$u_x = \sin \theta \cos \phi, \quad (2.17)$$

$$u_y = \sin \theta \sin \phi, \quad (2.18)$$

$$u_z = \cos \theta, \quad (2.19)$$

then in vector notation,

$$\mathbf{u} = -\mathbf{a}. \quad (2.20)$$

Then (2.16) can be written as

$$\tau_n = -\frac{1}{c} [u_x p_{x_n} + u_y p_{y_n} + u_z p_{z_n}] = -\frac{\mathbf{u}^T \mathbf{p}_n}{c}. \quad (2.21)$$

From (2.13), the n th component of $\mathbf{F}(\omega)$ is

$$F_n(\omega) = \int_{-\infty}^{\infty} e^{-j\omega t} f(t - \tau_n) dt = e^{-j\omega \tau_n} F(\omega), \quad (2.22)$$

where

$$\omega \tau_n = \frac{\omega}{c} \mathbf{a}^T \mathbf{p}_n = -\frac{\omega}{c} \mathbf{u}^T \mathbf{p}_n. \quad (2.23)$$

For plane waves propagating in a locally homogeneous medium, we define the wavenumber \mathbf{k} as

$$\mathbf{k} = \frac{\omega}{c} \mathbf{a} = \frac{2\pi}{\lambda} \mathbf{a}, \quad (2.24)$$

where λ is the wavelength corresponding to the frequency ω . Equivalently,

$$\mathbf{k} = -\frac{2\pi}{\lambda} \begin{bmatrix} \sin \theta \cos \phi \\ \sin \theta \sin \phi \\ \cos \theta \end{bmatrix} = -\frac{2\pi}{\lambda} \mathbf{u}. \quad (2.25)$$

The wave equation constrains the magnitude of the wavenumber,²

$$|\mathbf{k}| = \frac{\omega}{c} = \frac{2\pi}{\lambda}. \quad (2.26)$$

Therefore, only the direction of \mathbf{k} varies. Comparing (2.14) and (2.24), we observe that

$$\omega \tau_n = \mathbf{k}^T \mathbf{p}_n. \quad (2.27)$$

Defining

$$\mathbf{v}_k(\mathbf{k}) = \begin{bmatrix} e^{-j\mathbf{k}^T \mathbf{p}_0} \\ e^{-j\mathbf{k}^T \mathbf{p}_1} \\ \vdots \\ e^{-j\mathbf{k}^T \mathbf{p}_{N-1}} \end{bmatrix}, \quad (2.28)$$

²The wave equation is developed in a number of references (e.g., [Bal82]).

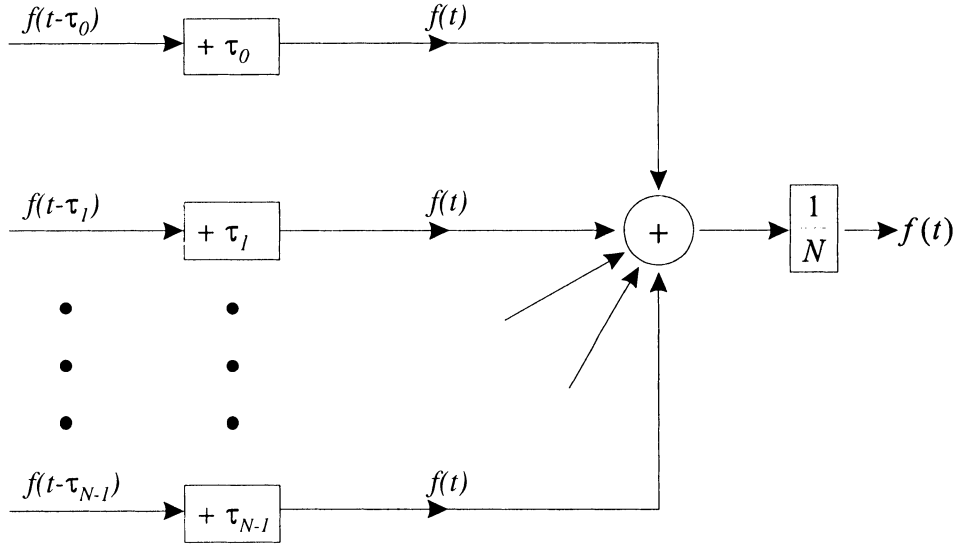


Figure 2.11 Delay-and-sum beamformer.

we can write $\mathbf{F}(\omega)$ as

$$\mathbf{F}(\omega) = F(\omega)\mathbf{v}_k(k). \quad (2.29)$$

The vector $\mathbf{v}_k(k)$ incorporates all of the spatial characteristics of the array and is referred to the **array manifold vector**. It plays a central role in our discussion. The subscript k denotes that the argument is in k -space. The subscript is to distinguish it from other variables we will use later as arguments to the array manifold vector.

In this case, we shift the inputs from each sensor so that the signals are aligned in time and add them. This operation is shown in Figure 2.11, where we have included a normalization factor $1/N$ so the output is $f(t)$. In this case,

$$h_n(\tau) = \frac{1}{N}\delta(\tau + \tau_n) \quad (2.30)$$

and

$$y(t) = f(t). \quad (2.31)$$

This processor is referred to as a **delay-and-sum beamformer** or the **conventional beamformer**. In practice we add a common delay in each channel so that the operations in Figure 2.11 are physically realizable.

Note that we can write (2.30) compactly in a matrix form in the frequency domain. If \mathbf{k}_s is the wavenumber of the plane-wave signal of interest, then

$$\mathbf{H}^T(\omega) = \frac{1}{N} \mathbf{v}_k^H(\mathbf{k}_s), \quad (2.32)$$

where $\mathbf{v}_k(\mathbf{k})$ was defined in (2.28).

Returning to the general problem, we want to find the response of the array to an input field $f(t, \mathbf{p})$. This can be done by the convolution and summing operation specified, but it is more useful to determine the response to a unit plane wave as a function of its temporal (radian) frequency ω and wavenumber \mathbf{k} . The systems theory approach of analyzing the response of a linear, time-invariant system in terms of the superposition of complex exponential basis functions can be extended to space-time signals.

The basis functions are now plane waves of the form,

$$f_n(t, \mathbf{p}_n) = \exp[j(\omega t - \mathbf{k}^T \mathbf{p}_n)], \quad n = 0, 1, \dots, N - 1, \quad (2.33)$$

or

$$\mathbf{f}(t, \mathbf{p}) = e^{j\omega t} \mathbf{v}_k(\mathbf{k}), \quad (2.34)$$

where $\mathbf{v}_k(\mathbf{k})$ was defined in (2.28).

The response of the array processor of (2.8) to a plane wave is

$$y(t, \mathbf{k}) = \mathbf{H}^T(\omega) \mathbf{v}_k(\mathbf{k}) e^{j\omega t}, \quad (2.35)$$

where $\mathbf{H}(\omega)$ is the Fourier transform of $\mathbf{h}(\tau)$ in (2.9).

We emphasize the dependence of the output upon the input wavenumber \mathbf{k} with the notation $y(t, \mathbf{k})$. The temporal dependence is a complex exponential at the same frequency as the input plane wave. Equation (2.35) can be written in the frequency domain as

$$Y(\omega, \mathbf{k}) = \mathbf{H}^T(\omega) \mathbf{v}_k(\mathbf{k}). \quad (2.36)$$

Note that ω is a single frequency corresponding to the input frequency. The temporal spatial processing by the array is completely described by the term on the right side of (2.36). We define this term as

$\Upsilon(\omega, \mathbf{k}) \triangleq \mathbf{H}^T(\omega) \mathbf{v}_k(\mathbf{k}),$

(2.37)

which we term the **frequency-wavenumber response function** of the array. It describes the complex gain of an array to an input plane wave with wavenumber \mathbf{k} and temporal frequency ω , and has the same interpretation as

a transfer function for a linear time-invariant system (we introduce $\Upsilon(\omega, \mathbf{k})$ because $Y(\omega, \mathbf{k})$ will be used later to describe the output due to arbitrary inputs). $\Upsilon(\omega, \mathbf{k})$ is defined over the entire \mathbf{k} space. The second term in (2.37), $\mathbf{v}_k(\mathbf{k})$, is the array manifold vector defined in (2.28).

The frequency-wavenumber response function describes the response to an arbitrary plane wave. In most physical applications there is a coupling between the temporal frequency ω and the spatial wavenumber \mathbf{k} through the wave equation governing the propagation of the plane wave. Sometimes this can be a very simple relationship such as a plane wave in a homogeneous (and infinite) space; in other instances it can be quite complicated, such as the modal behavior in layered media that often occurs in underwater acoustics and seismology.

The **beam pattern** for an array is defined in the context of plane waves propagating in a locally homogeneous medium where one has the wave equation constraint given in (2.26). This constrains the magnitude of the wavenumber \mathbf{k} as given in (2.26). The beam pattern is the frequency-wavenumber response function evaluated versus the direction, or

$$B(\omega : \theta, \phi) = \Upsilon(\omega, \mathbf{k})|_{\mathbf{k}=\frac{2\pi}{\lambda} \mathbf{a}(\theta, \phi)}, \quad (2.38)$$

where $\mathbf{a}(\theta, \phi)$ is a unit vector with spherical coordinate angles θ, ϕ . We see that the beam pattern is the frequency-wavenumber function evaluated on a sphere of radius $2\pi/\lambda$.

The beam pattern of an array is a key element in determining the array performance. In the next section, we develop the beam patterns for a uniformly weighted linear array.

In the text, we emphasize the case in which the $f(t, \mathbf{p}_n)$ are bandpass signals,

$$f(t, \mathbf{p}_n) = \sqrt{2} \Re e \left\{ \tilde{f}(t, \mathbf{p}_n) e^{j\omega_c t} \right\}, \quad n = 0, \dots, N - 1, \quad (2.39)$$

where ω_c is the carrier frequency and $\tilde{f}(t, \mathbf{p}_n)$ is the complex envelope. We assume that the complex envelope is bandlimited to the region,

$$|\omega_L| \leq 2\pi B_s / 2, \quad (2.40)$$

where

$$\omega_L \triangleq \omega - \omega_c, \quad (2.41)$$

and πB_s is a constant specifying the maximum bandwidth of the complex envelope.

For the plane wave in (2.13), (2.39) becomes

$$f(t, \mathbf{p}_n) = \sqrt{2} \operatorname{Re} \left\{ \tilde{f}(t - \tau_n) e^{j\omega_c(t - \tau_n)} \right\}, \quad n = 0, \dots, N - 1, \quad (2.42)$$

where τ_n is given by (2.21).

We now consider the travel time across the array. We define $\Delta T_{nm}(\mathbf{u})$ as the travel time between the n and m elements for a plane wave whose directional cosine is \mathbf{u} . Then,

$$\Delta T_{max} \triangleq \max_{n,m=0,\dots,N-1;\mathbf{u}} \{\Delta T_{nm}(\mathbf{u})\}, \quad (2.43)$$

is the maximum travel time between any two elements in the array. For a linear array it would be the travel time between the two elements at the ends of the array for a signal arriving along the array axis (endfire).

We assume that the origin is located at the center of gravity of the array,

$$\sum_{n=0}^{N-1} \mathbf{p}_n = \mathbf{0}; \quad (2.44)$$

then all of the τ_n in (2.13) satisfy

$$\tau_n \leq \Delta T_{max}, \quad n = 0, \dots, N - 1. \quad (2.45)$$

In many cases of interest, the bandwidth of the complex envelope is small enough that

$$\tilde{f}(t - \tau_n) \simeq \tilde{f}(t), \quad n = 0, 1, \dots, N - 1. \quad (2.46)$$

In order for this approximation to be valid, we require

$$B_s \cdot \Delta T_{max} \ll 1. \quad (2.47)$$

We define bandpass signals whose complex envelopes satisfy (2.47) as **narrowband** signals. Later we will revisit this definition in the context of optimum processors and provide a better quantitative discussion. For the present, we use (2.47). Then (2.42) reduces to

$$f(t, \mathbf{p}_n) = \sqrt{2} \operatorname{Re} \left\{ \tilde{f}(t) e^{-j\omega_c \tau_n} e^{j\omega_c t} \right\}. \quad (2.48)$$

We see that, in the narrowband case, the delay is approximated by a phase shift. Therefore the delay-and-sum beamformer can be implemented by a set of phase shifts instead of delay lines. The resulting beamformer is shown in Figure 2.12. This implementation is commonly referred to as a **phased array** and is widely used in practice.

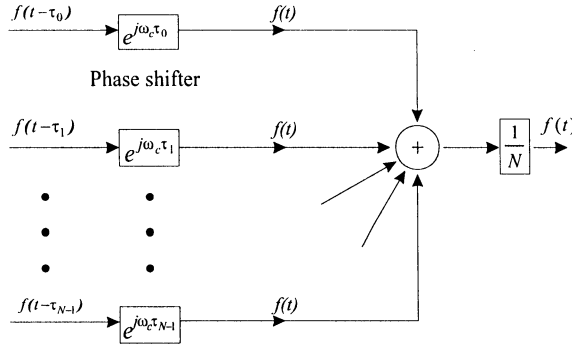


Figure 2.12 Narrowband beamformer implemented using phase shifters.

We will find that, in many applications, we want to adjust the gain and phase at the output of each sensor to achieve a desirable beam pattern. This leads to the narrowband model shown in Figure 2.13(a). The w_n^* are complex weights that are implemented as a cascade of a gain and phase shifter, as shown in Figure 2.13(b).

An alternative implementation is shown in Figure 2.13(c). In some cases, we implement the beamformer by performing a quadrature demodulation and applying the complex weights at baseband. We actually apply $\text{Re}[w_n^*]$ to one quadrature component and $\text{Im}[w_n^*]$ to the other quadrature component. The results are identical. We discuss these cases later in the text.

Defining the complex weight vector as

$$\mathbf{w}^H = [w_0^* \ w_1^* \ \cdots \ w_{N-1}^*], \quad (2.49)$$

(2.35) becomes

$$y(t, \mathbf{k}) = \mathbf{w}^H \mathbf{v}_k(\mathbf{k}) e^{j\omega t}, \quad (2.50)$$

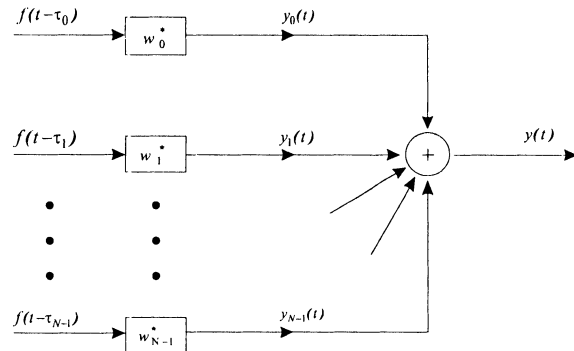
and

$$\Upsilon(\omega, \mathbf{k}) = \mathbf{w}^H \mathbf{v}_k(\mathbf{k}). \quad (2.51)$$

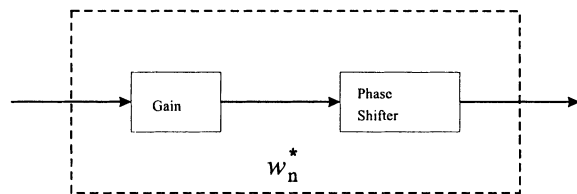
The definition in (2.49) is equivalent to

$$\mathbf{w}^H = \mathbf{H}^T(\omega_c). \quad (2.52)$$

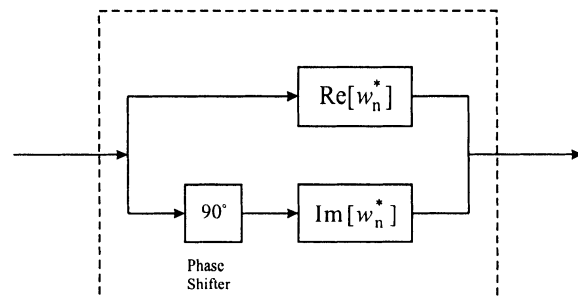
The majority of the text focuses on the narrowband model. In Chapter 5, we show that one approach to processing broadband signals is to decompose them into narrower frequency bins by a discrete Fourier transform (DFT). Within each bin, the narrowband condition is satisfied and all of our narrowband results can be used directly.



(a)

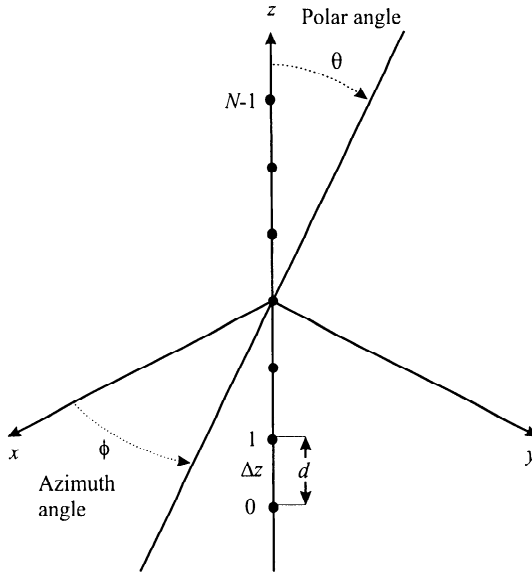


(b)



(c)

Figure 2.13 General narrowband beamformer.

Figure 2.14 Linear array along z -axis.

2.3 Uniform Linear Arrays

The linear array of interest is shown in Figure 2.14. There are N elements located on the z -axis with uniform spacing equal to d . We refer to this type of array as a **uniform linear array (ULA)**. We have placed the center of the array at the origin of the coordinate system. This centering will lead to computational advantages and will be used throughout the text.

The locations of the elements are

$$p_{z_n} = \left(n - \frac{N-1}{2} \right) d, \quad n = 0, 1, \dots, N-1, \quad (2.53)$$

and

$$p_{x_n} = p_{y_n} = 0. \quad (2.54)$$

To find the array manifold vector $\mathbf{v}_k(k)$, we substitute (2.53) and (2.54) into (2.28) to obtain

$$\mathbf{v}_k(k_z) = \left[e^{j(\frac{N-1}{2})k_z d} \mid e^{j(\frac{N-1}{2}-1)k_z d} \mid \dots \mid e^{-j(\frac{N-1}{2})k_z d} \right]^T, \quad (2.55)$$

with

$$k_z = -\frac{2\pi}{\lambda} \cos \theta = -k_0 \cos \theta, \quad (2.56)$$

where

$$k_0 \triangleq |\mathbf{k}| \triangleq \frac{2\pi}{\lambda} \quad (2.57)$$

is the magnitude of the wavenumber. Note that the linear array has no resolution capability in the ϕ -direction. Using (2.49) and (2.55) in (2.51) gives

$$\begin{aligned} \Upsilon(\omega, k_z) &= \mathbf{w}^H \mathbf{v}_k(k_z) \\ &= \sum_{n=0}^{N-1} w_n^* e^{-j(n-\frac{N-1}{2})k_z d}. \end{aligned} \quad (2.58)$$

We will also find it useful to define

$$\psi = -k_z d = \frac{2\pi}{\lambda} \cos \theta \cdot d = \frac{2\pi}{\lambda} u_z d, \quad (2.59)$$

where u_z is the directional cosine with respect to the z -axis,

$$u_z = \cos \theta. \quad (2.60)$$

Using (2.59) in (2.58) gives

$$\Upsilon_\psi(\psi) = e^{-j\frac{N-1}{2}\psi} \sum_{n=0}^{N-1} w_n^* e^{jn\psi}. \quad (2.61)$$

We refer to $\Upsilon_\psi(\psi)$ as the frequency-wavenumber function in ψ -space. Both $\Upsilon(\omega, k_z)$ and $\Upsilon_\psi(\psi)$ are defined from $-\infty$ to ∞ , but they only represent propagating signals in the region where $0 \leq \theta \leq \pi$ (or $-1 \leq u_z \leq 1$). This restriction implies $-\frac{2\pi d}{\lambda} \leq \psi \leq \frac{2\pi d}{\lambda}$ or $-\frac{2\pi}{\lambda} \leq k_z \leq \frac{2\pi}{\lambda}$. We refer to this as the **visible region**.

We observe that, if we define

$$z = e^{j\psi}, \quad (2.62)$$

$$\Upsilon_z(z) = z^{-\frac{N-1}{2}} \sum_{n=0}^{N-1} w_n^* z^n, \quad (2.63)$$

then (2.63) can be written as

$$\Upsilon_z(z) = z^{-\frac{N-1}{2}} \left(\sum_{n=0}^{N-1} w_n z^{-n} \right)^*. \quad (2.64)$$

The term

$$W(z) = \sum_{n=0}^{N-1} w_n z^{-n} \quad (2.65)$$

is familiar as the z -transform³ and

$$\Upsilon_\psi(\psi) = \Upsilon_z(z)|_{z=e^{j\psi}} = \left(z^{-\frac{N-1}{2}} W^*(z) \right) \Big|_{z=e^{j\psi}} \quad (2.66)$$

is the frequency-wavenumber function in ψ -space. We exploit this relationship later in the text.

Although it may appear that we have introduced extra notation by writing the frequency-wavenumber function in three different ways ((2.58), (2.61) and (2.66)), we will find the different forms useful in different cases.

It is also useful to define the array manifold vector in θ and u space,

$$[\mathbf{v}_\theta(\theta)]_n = e^{j(n-\frac{N-1}{2})\frac{2\pi d}{\lambda} \cos \theta}, \quad n = 0, \dots, N-1, \quad (2.67)$$

and

$$[\mathbf{v}_u(u)]_n = e^{j(n-\frac{N-1}{2})\frac{2\pi d}{\lambda} u}, \quad n = 0, \dots, N-1. \quad (2.68)$$

We can also write the beam pattern in three forms. The key difference between the frequency-wavenumber function and the beam pattern is that the argument in the beam pattern is restricted to correspond to a physical angle θ . Thus,

$$B_\theta(\theta) = \mathbf{w}^H \mathbf{v}_\theta(\theta) = e^{-j(\frac{N-1}{2})\frac{2\pi d}{\lambda} \cos \theta} \sum_{n=0}^{N-1} w_n^* e^{jn\frac{2\pi d}{\lambda} \cos \theta}, \quad 0 \leq \theta \leq \pi, \quad (2.69)$$

$$B_u(u) = \mathbf{w}^H \mathbf{v}_u(u) = e^{-j(\frac{N-1}{2})\frac{2\pi d}{\lambda} u} \sum_{n=0}^{N-1} w_n^* e^{jn\frac{2\pi d}{\lambda} u}, \quad -1 \leq u \leq 1, \quad (2.70)$$

$$B_\psi(\psi) = \mathbf{w}^H \mathbf{v}_\psi(\psi) = e^{-j(\frac{N-1}{2})\psi} \sum_{n=0}^{N-1} w_n^* e^{jn\psi}, \quad -\frac{2\pi d}{\lambda} \leq \psi \leq \frac{2\pi d}{\lambda}. \quad (2.71)$$

We suppress the subscript on $B(\cdot)$ when the variable is clear.

For uniform linear arrays, we normally write the array manifold vector in terms of ψ ,

$$[\mathbf{v}_\psi(\psi)]_n = e^{j(n-\frac{N-1}{2})\psi}, \quad n = 0, 1, \dots, N-1, \quad (2.72)$$

³The z -transform is discussed in a number of texts (e.g., Chapter 4 of [OS89]).

and

$$\mathbf{v}_\psi(\psi) = \begin{bmatrix} e^{-j(\frac{N-1}{2})\psi} & e^{-j(\frac{N-3}{2})\psi} & \dots & e^{j(\frac{N-3}{2})\psi} & e^{j(\frac{N-1}{2})\psi} \end{bmatrix}^T. \quad (2.73)$$

We see that the array manifold vector for a uniform linear array exhibits a **conjugate symmetry**. For N even, if we define a $N/2$ -dimensional vector $\mathbf{v}_{\psi_1}(\psi)$ corresponding to the first $N/2$ elements of $\mathbf{v}_\psi(\psi)$, then we can write

$$\mathbf{v}_\psi(\psi) = \begin{bmatrix} \mathbf{v}_{\psi_1}(\psi) \\ \mathbf{J} \mathbf{v}_{\psi_1}^*(\psi) \end{bmatrix}, \quad (2.74)$$

where \mathbf{J} is the exchange matrix defined in (A.125). For N odd, $\mathbf{v}_{\psi_1}(\psi)$ consists of the first $(N-1)/2$ elements and

$$\mathbf{v}_\psi(\psi) = \begin{bmatrix} \mathbf{v}_{\psi_1}(\psi) \\ 1 \\ \mathbf{J} \mathbf{v}_{\psi_1}^*(\psi) \end{bmatrix}. \quad (2.75)$$

This conjugate symmetry will lead to computational savings and performance improvements in many applications. For example, if \mathbf{w} is also conjugate symmetric, we can write, for N even,

$$\mathbf{w} = \begin{bmatrix} \mathbf{w}_1 \\ \mathbf{J} \mathbf{w}_1^* \end{bmatrix}. \quad (2.76)$$

The beam pattern in ψ -space is,

$$\begin{aligned} B_\psi(\psi) &= \mathbf{w}^H \mathbf{v}_\psi(\psi) \\ &= [\mathbf{w}_1^H \mid \mathbf{w}_1^T \mathbf{J}] \begin{bmatrix} \mathbf{v}_{\psi_1}(\psi) \\ \mathbf{J} \mathbf{v}_{\psi_1}^*(\psi) \end{bmatrix} \\ &= \mathbf{w}_1^H \mathbf{v}_{\psi_1}(\psi) + \mathbf{w}_1^T \mathbf{v}_{\psi_1}^*(\psi) \\ &= 2\operatorname{Re} [\mathbf{w}_1^H \mathbf{v}_{\psi_1}(\psi)], \end{aligned} \quad (2.77)$$

so the beam pattern is a real function. Note that if we have real symmetric weightings, then (2.76) is also satisfied. A similar result follows for N

odd. Later, we will find that many other array geometries exhibit conjugate symmetry.

The form in (2.73) emphasizes the conjugate symmetry in $\mathbf{v}_\psi(\psi)$. We can also write $\mathbf{v}_\psi(\psi)$ as

$$\mathbf{v}_\psi(\psi) = e^{-j\frac{N-1}{2}\psi} \begin{bmatrix} 1 & e^{j\psi} & \dots & e^{j(N-1)\psi} \end{bmatrix}^T. \quad (2.78)$$

This form emphasizes the Vandermonde structure (A.163) of $\mathbf{v}_\psi(\psi)$.

In Chapter 3, we develop techniques for choosing \mathbf{w} in order to achieve a beam pattern with desirable properties. This is the most common approach. However, we will also develop techniques for synthesizing a desirable $B_\psi(\psi)$ without finding \mathbf{w} in the process. Thus, our last step is to find the \mathbf{w} that corresponds to a particular $B_\psi(\psi)$.

We start with the relation in (2.71),

$$B_\psi(\psi) = \mathbf{w}^H \mathbf{v}_\psi(\psi). \quad (2.79)$$

We assume that $B_\psi(\psi)$ is known and we want to find the \mathbf{w} that generated it. Since \mathbf{w}^H is a $1 \times N$ vector, we would anticipate that, if we know the value of $B_\psi(\psi)$ at N values of ψ , we can find \mathbf{w} .

We sample the beam pattern at N values of $\psi_i, i = 1, \dots, N$. The ψ_i must be distinct but do not have to be spaced equally. We denote the beam pattern at the sample points as $B(\psi_i)$. From (2.79),

$$\mathbf{w}^H \mathbf{v}(\psi_i) = B(\psi_i), \quad i = 1, \dots, N. \quad (2.80)$$

We define an $N \times N$ array manifold matrix,

$$\mathbf{V}(\psi) \triangleq \begin{bmatrix} \mathbf{v}(\psi_1) & \dots & \mathbf{v}(\psi_N) \end{bmatrix}, \quad (2.81)$$

and a $1 \times N$ beam pattern matrix,

$$\mathbf{B} \triangleq \begin{bmatrix} B(\psi_1) & \dots & B(\psi_N) \end{bmatrix}. \quad (2.82)$$

Then, (2.80) can be written as

$$\mathbf{w}^H \mathbf{V}(\psi) = \mathbf{B}, \quad (2.83)$$

or

$$\mathbf{V}^H(\psi) \mathbf{w} = \mathbf{B}^H. \quad (2.84)$$

Since $\mathbf{V}^H(\psi)$ is full rank,

$$\boxed{\mathbf{w} = [\mathbf{V}^H(\psi)]^{-1} \mathbf{B}^H},$$

(2.85)

which is the desired result. Although the ψ_i are arbitrary, if they are too close, the array manifold vectors will approach linear dependence and there may be numerical problems with the inverse in (2.85). If we use uniform spacing of $2\pi/N$, we will derive an algorithm in Section 3.3 that is computationally more efficient.

A particular of interest is the case in which we have specified the beam pattern with $N - 1$ zeros. If we assume the array is steered to broadside, we let

$$\psi_1 = 0, \quad (2.86)$$

and $\psi_2, \psi_3, \dots, \psi_N$ correspond to the zero locations. Assuming a normalized beam pattern,

$$\mathbf{B} = \begin{bmatrix} 1 & 0 & \cdots & 0 \end{bmatrix} = \mathbf{e}_1^T. \quad (2.87)$$

Then, (2.85) reduces to

$$\boxed{\mathbf{w} = \left[\mathbf{V}^H(\psi) \right]^{-1} \mathbf{e}_1}. \quad (2.88)$$

We will find these algorithms to be very useful in subsequent sections.

There are two points with the results in (2.85) and (2.88) that should be emphasized:

- (i) We have assumed that $B_\psi(\psi)$ was defined by (2.79). In other words, it was generated by a complex $N \times 1$ vector \mathbf{w} . If we start with an arbitrary function $B_\psi(\psi)$ and use (2.85), we will generate a pattern that matches $B(\psi_i)$, $i = 1, \dots, N$ but will not necessarily match the function $B_\psi(\psi)$. We discuss this issue further in Section 3.3.
- (ii) We introduced this result in the context of a uniform linear array. However, the derivation is valid for an N -element array with an arbitrary geometry.

We have developed the basic relationships between the array manifold vector, the weight vector, and the beam pattern. In the next section, we consider the special case of uniform weighting.

2.4 Uniformly Weighted Linear Arrays

We now restrict our attention to the uniform weighting case,

$$w_n = \frac{1}{N}, \quad n = 0, 1, \dots, N - 1. \quad (2.89)$$

We can also write (2.89) as

$$\mathbf{w} = \frac{1}{N} \mathbf{1}, \quad (2.90)$$

where $\mathbf{1}$ is the $N \times 1$ unity vector defined in Section A.3.1.

Thus, the frequency-wavenumber function can be written in ψ -space as⁴

$$\begin{aligned} \Upsilon_\psi(\psi) &= \frac{1}{N} \sum_{n=0}^{N-1} e^{j(n-\frac{N-1}{2})\psi} \\ &= \frac{1}{N} e^{-j(\frac{N-1}{2})\psi} \sum_{n=0}^{N-1} e^{j n \psi} \\ &= \frac{1}{N} e^{-j(\frac{N-1}{2})\psi} \left[\frac{1 - e^{j N \psi}}{1 - e^{j \psi}} \right], \end{aligned} \quad (2.91)$$

or

$$\Upsilon_\psi(\psi) = \frac{1}{N} \frac{\sin\left(N\frac{\psi}{2}\right)}{\sin\frac{\psi}{2}}, \quad -\infty < \psi < \infty. \quad (2.92)$$

We observe that $\Upsilon_\psi(\psi)$ is periodic with period 2π for N odd. If N is even, the lobes at $\pm 2\pi, \pm 6\pi$ are negative and period is 4π . The period of $|\Upsilon_\psi(\psi)|$ is 2π for any value of N . $\Upsilon_\psi(\psi)$ is plotted versus ψ in Figure 2.15 for $N = 11$. In Figure 2.16, we plot $|\Upsilon_\psi(\psi)|$ in dB, where

$$\Upsilon_{dB}(\psi) = 10 \log_{10} |\Upsilon(\psi)|^2. \quad (2.93)$$

For arbitrary \mathbf{w} , $\Upsilon_\psi(\psi)$ is complex, so the phase should also be plotted; however, the symmetry of this particular array leads to a purely real quantity.

We can also write the frequency-wavenumber response in terms of k_z ,

$$\Upsilon(\omega : k_z) = \frac{1}{N} \frac{\sin\left(N k_z \frac{d}{2}\right)}{\sin\left(k_z \frac{d}{2}\right)}. \quad (2.94)$$

$\Upsilon(\omega : k_z)$ is periodic with period $2\pi/d$.

Note that the response function depends only upon the wavenumber component k_z and is periodic with respect to k_z at intervals of $2\pi/d$. The dependence solely upon k_z is a consequence of the linear array being one-dimensional so it can only resolve wavenumber components which have a projection in this direction.

⁴ $\sum_{n=0}^{N-1} x^n = \frac{1-x^N}{1-x}$.

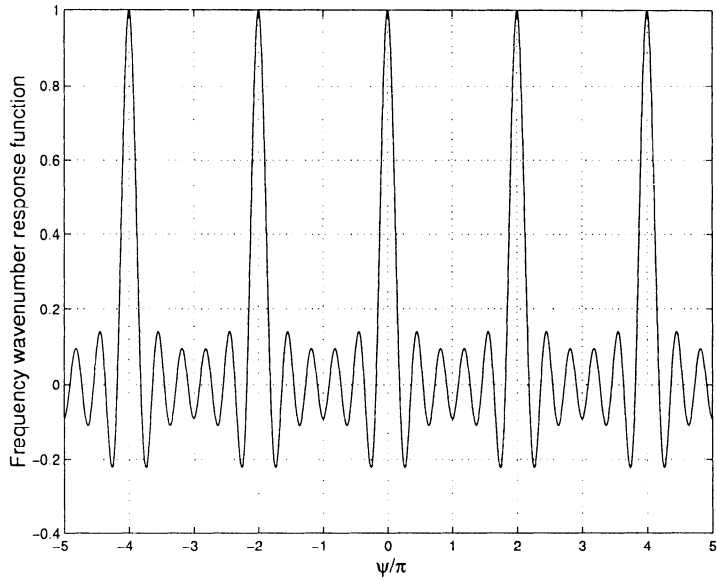


Figure 2.15 $\Upsilon(\psi) : \psi = \frac{2\pi}{\lambda} d \cos \theta, N = 11.$

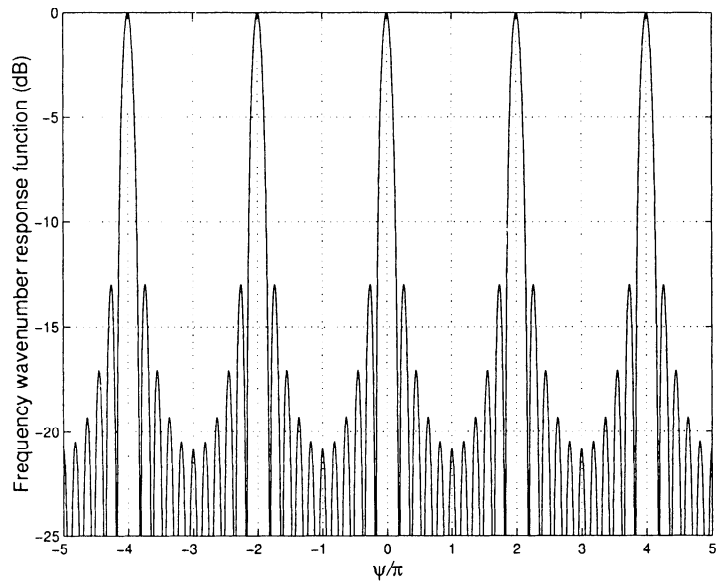
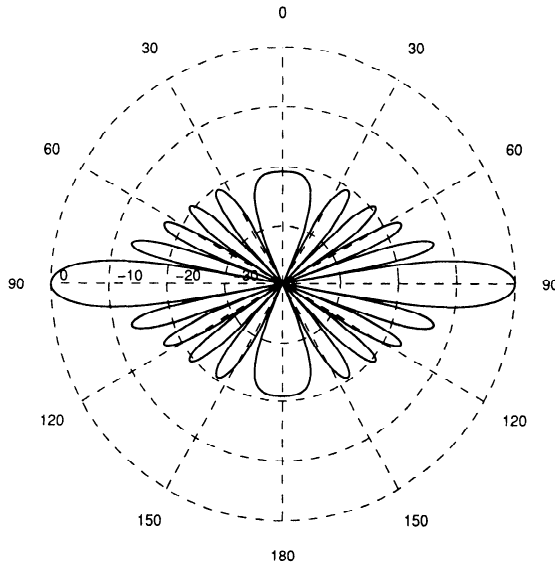


Figure 2.16 $|\Upsilon(\psi)|$ in dB.

Figure 2.17 Polar plot of $B_\theta(\theta)$.

The beam pattern is given by

$$B_\theta(\theta) = \frac{1}{N} \frac{\sin\left(\frac{N}{2} \cdot \frac{2\pi}{\lambda} \cos \theta \cdot d\right)}{\sin\left(\frac{1}{2} \cdot \frac{2\pi}{\lambda} \cos \theta \cdot d\right)}, \quad 0 \leq \theta \leq \pi. \quad (2.95)$$

The beam pattern in u -space can be written as

$$B_u(u) = \frac{1}{N} \frac{\sin\left(\frac{\pi N d}{\lambda} u\right)}{\sin\left(\frac{\pi d}{\lambda} u\right)}, \quad -1 \leq u \leq 1. \quad (2.96)$$

The beam pattern is only defined over the region $(-1 \leq u \leq 1)$, the **visible region**. The beam pattern in ψ -space is

$$B_\psi(\psi) = \frac{1}{N} \frac{\sin\left(N \frac{\psi}{2}\right)}{\sin\left(\frac{\psi}{2}\right)}, \quad -\frac{2\pi d}{\lambda} \leq \psi \leq \frac{2\pi d}{\lambda}. \quad (2.97)$$

The functions $B_u(u)$ and $B_\psi(\psi)$ are sometimes referred to as the **array factor**. We will see the significance of this term when we look at non-isotropic sensors.

In Figure 2.17, we show a polar plot in dB of $B_\theta(\theta)$. If we plotted the beam pattern in three dimensions, the plot in Figure 2.17 would correspond

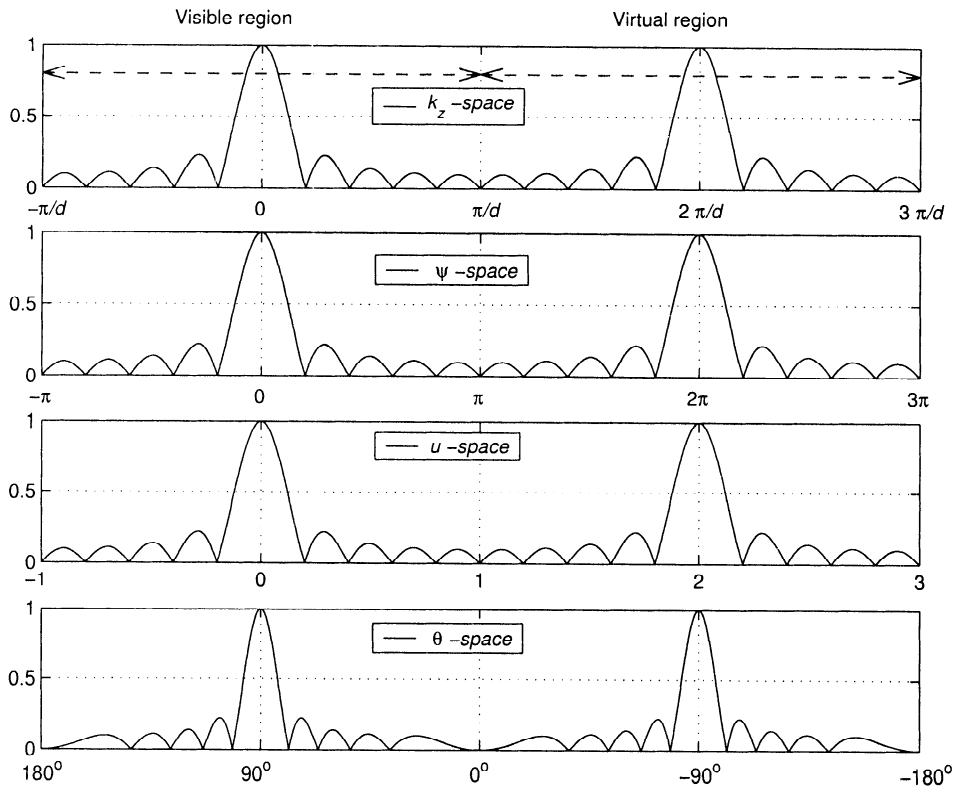


Figure 2.18 $|\Upsilon_\psi(\psi)|$ for a linear array with $d = \lambda/2$ and $N = 10$.

to a pattern cut along any value of ϕ , the azimuth angle. In Figure 2.18, we show the magnitude of the beam pattern versus different variables.

Although this is a simple example, we can use it to illustrate several important characteristics of linear arrays. The first set of characteristics describe the parameters of the beam pattern.

2.4.1 Beam Pattern Parameters

- (i) 3-dB beamwidth (the half-power beamwidth, HPBW)
- (ii) Distance to first null (twice this distance is BW_{NN})
- (iii) Distance to first sidelobe
- (iv) Height of first sidelobe
- (v) Location of remaining nulls
- (vi) Rate of decrease of sidelobes
- (vii) Grating lobes

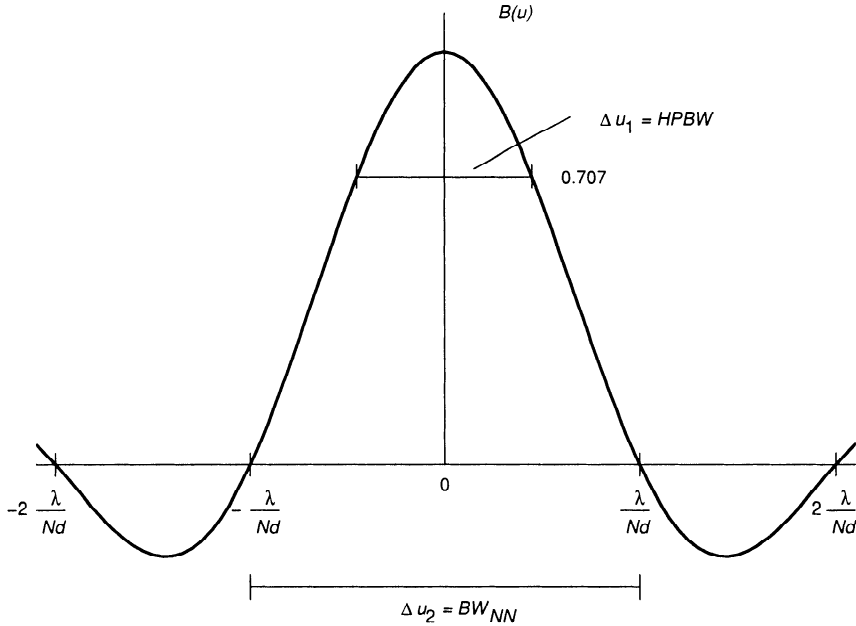


Figure 2.19 Main lobe of beam pattern.

To illustrate the first two points, consider the beam pattern near the origin as shown in Figure 2.19.

The 3-dB beamwidth is a measure of the width of the beam. It is defined to be the point where $|B_u(u)|^2 = 0.5$ or $|B_u(u)| = 1/\sqrt{2}$. We can find the half-power point in u -space by setting $B_u(u)$ in (2.96) equal to $1/\sqrt{2}$. Calculating this value as N increases, we find that, for $N \geq 10$, a good approximation is obtained by solving the equation,

$$\frac{\pi N d}{\lambda} u = 1.4 \quad (2.98)$$

(see Problem 2.4.7). Then,

$$\frac{\Delta u_1}{2} = 1.4 \frac{\lambda}{\pi N d} \quad (2.99)$$

or

$$\Delta u_1 = 0.891 \frac{\lambda}{N d}. \quad (2.100)$$

We refer to this interval as the **half-power beamwidth (HPBW)**. As N increases, the coefficient in (2.100) reduces slightly. For $N > 30$, $0.886\lambda/Nd$ is a better approximation.

The HPBWs in terms of the various spaces are listed in Table 2.2.

Table 2.2 HPBWs in Various Spaces

Space	Arbitrary d	$d = \lambda/2$
u	$0.891 \frac{\lambda}{Nd}$	$1.782 \frac{1}{N}$
$\bar{\theta}$	$2\sin^{-1}(0.446 \frac{\lambda}{Nd})$	$2\sin^{-1}(0.891 \frac{1}{N})$
small $\bar{\theta}$	$\simeq 0.891 \frac{\lambda}{Nd}$ radians $\simeq 51.05 \frac{\lambda}{Nd}$ degrees	$\simeq 1.782 \frac{1}{N}$ radians $\simeq 102.1 \frac{1}{N}$ degrees
ψ	$0.891 \frac{2\pi}{N}$	$0.891 \frac{2\pi}{N}$
k_z	$0.891 \frac{2\pi}{dN}$	$1.782 \frac{2\pi}{\lambda N}$

We define $\bar{\theta} = \pi/2 - \theta$ as the angle measured from broadside (see Figure 2.2).

The nulls of the pattern occur when the numerator of $B_u(u)$ is zero and the denominator is non-zero:

$$\sin\left(\frac{\pi Nd}{\lambda}u\right) = 0, \quad (2.101)$$

when

$$\frac{\pi Nd}{\lambda}u = m\pi, \quad m = 1, 2, \dots \quad (2.102)$$

Thus the nulls occur when both

$$u = m \frac{\lambda}{Nd}, \quad m = 1, 2, \dots, \quad (2.103)$$

and

$$u \neq m \frac{\lambda}{d}, \quad m = 1, 2, \dots. \quad (2.104)$$

Thus, the first null occurs at λ/Nd and

$$\Delta u_2 = 2 \frac{\lambda}{Nd}. \quad (2.105)$$

We refer to Δu_2 as the null-to-null beamwidth and denote it by BW_{NN} . One-half of the BW_{NN} is the distance to the first null ($0.5BW_{NN}$). This quantity provides a measure of the ability of the array to resolve two different plane waves. It is referred to as the **Rayleigh resolution limit**. Two plane waves are considered resolvable if the peak of the second beam pattern lies at or outside of the null of the first beam pattern (separation $\geq \Delta u_2/2$). Later, we look at statistical measures of an array's resolution capability.

Note that the linear array has no resolution capability in the azimuthal direction (ϕ) because it has no extent in either the x or y directions. We will discuss the resolution problem in detail in later sections.

The BW_{NN} in terms of the various spaces is listed in Table 2.3.

Table 2.3 BW_{NN} in Various Spaces

Space	Arbitrary d	$d = \lambda/2$
u	$2\frac{\lambda}{Nd}$	$\frac{4}{N}$
$\bar{\theta}$	$2\sin^{-1}\left(\frac{\lambda}{Nd}\right)$	$2\sin^{-1}\left(\frac{2}{N}\right)$
small $\bar{\theta}$	$\simeq 2\frac{\lambda}{Nd}$ radians	$\simeq \frac{4}{N}$ radians
ψ	$\frac{4\pi}{N}$	$\frac{4\pi}{N}$
k_z	$\frac{4\pi}{dN}$	$\frac{8\pi}{\lambda N}$

2.4.1.1 Location of sidelobes and the rate of decrease

The location of the maxima of the sidelobes occurs approximately when the numerator of (2.96) is a maximum:

$$\sin\left(\frac{N\psi}{2}\right) = 1. \quad (2.106)$$

Thus,

$$\frac{N\psi}{2} = \pm(2m+1)\frac{\pi}{2}, \quad m = 1, 2, \dots \quad (2.107)$$

or

$$\psi = \pm\frac{2m+1}{N}\pi \quad (2.108)$$

and

$$u = \pm\frac{2m+1}{N}\frac{\lambda}{2d}. \quad (2.109)$$

The peak of the first sidelobe occurs at

$$\psi = \pm\frac{3\pi}{N}. \quad (2.110)$$

Since the numerator in (2.97) is approximately one at the maximum, the value at the maximum is given by

$$B_\psi\left(\pm\frac{3\pi}{N}\right) \cong \frac{1}{N \sin(\frac{3\pi}{2N})}. \quad (2.111)$$

For large N , this can be further approximated by

$$B_\psi \left(\pm \frac{3\pi}{N} \right) \cong \frac{2}{3\pi} \quad (2.112)$$

or -13.5 dB. This implies that a signal 13.5 dB higher at these sidelobe locations would produce the same response as one at $k_z = 0$. The major sidelobes appear at $k_z = \pm(2m + 1)\pi/Nd$ and the levels diminish as $1/(2m + 1)$. For example, the next highest sidelobes are -17.9 dB. In practice this level of discrimination is generally not acceptable, so uniformly weighted arrays are seldom used. The issue of sidelobe control is especially important in both deterministic and adaptive array designs. We discuss the deterministic case in Chapter 3 and the adaptive case in Chapter 7.

2.4.1.2 Grating lobes

In Figure 2.20, we plot $|\Upsilon_u(u)|$ for various values of d/λ . It illustrates the important concept of “grating lobe,” which is a lobe of the same height as the main lobe. Grating lobes occur when both the numerator and denominator of (2.97) equals one. These appear at intervals,

$$\frac{\psi}{2} = m \cdot \pi, \quad (2.113)$$

or

$$\psi = m \cdot 2\pi, \quad (2.114)$$

or

$$u = m \cdot \frac{\lambda}{d}. \quad (2.115)$$

If the array spacing is greater than λ , then the peak of the grating lobe occurs within the region of propagating signals, that is, when $|u| \leq 1$. Here one has an ambiguity in terms of the peak response and only *a priori* information about the direction of the signal can resolve it.

In the next section, we discuss array steering. We find that steering causes the frequency-wavenumber function in u -space, $\Upsilon_u(u)$, to shift in u -space. This shift causes grating lobes to move into the visible region. We find that, if the array is required to steer $0^\circ \leq \theta \leq 180^\circ$, then we require,

$$\frac{d}{\lambda} \leq \frac{1}{2}, \quad (2.116)$$

or

$$d \leq \frac{\lambda}{2}. \quad (2.117)$$

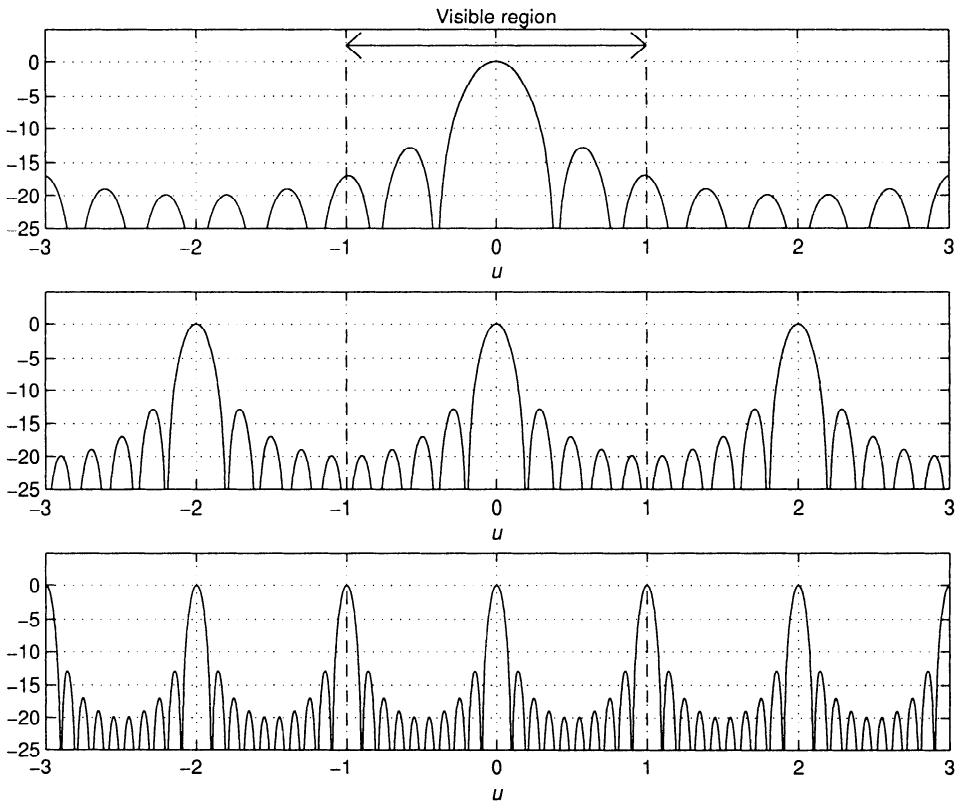


Figure 2.20 Effect of element spacing on beam pattern: (a) $d = \lambda/4$; (b) $d = \lambda/2$; (c) $d = \lambda$.

Normally, we consider arrays where $d \leq \lambda/2$ and assume that steering over the entire sphere is required. We refer to a uniform linear array with $d = \lambda/2$ as a **standard linear array**.

The problem of grating lobes is identical to the problem of aliasing in time series analysis, which occurs when we undersample the time domain waveform.

2.5 Array Steering

The discussions in Sections 2.2, 2.3, and 2.4 have considered arrays whose maximum response axis was at broadside, or $k_z = 0$. In most applications we want to be able to position, or steer, the response to an arbitrary wavenumber, or direction. There are two ways to accomplish this. The

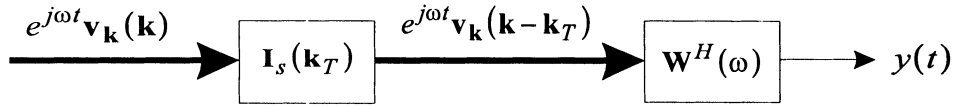


Figure 2.21 Array steering with delays.

direct approach is to change the location of the sensors so that the axis is perpendicular to the desired steering direction. This is termed mechanical steering, and this is what is being done when an antenna is physically rotated such as a parabolic aperture in a radar system. Often mechanical steering is not possible because of either the large physical dimensions of an array when operating with long wavelength signals or the need to recalibrate sensors when they are moved.

An alternative approach is to introduce time delays (or in the narrow-band case, phase shifts) to steer the **main response axis (MRA)** of an array. This is termed electronic steering. With the advances in very high speed signal processors, electronic steering is being used much more extensively in array processing, not only because of the restrictions of mechanical steering but also because of its flexibility and its ability to change the response function rapidly. In some arrays we use mechanical steering in one direction and electronic steering in the other direction.

We first consider an arbitrary array and then specialize our results to a uniformly weighted array.

Our simple example at the beginning of Section 2.2 illustrated the idea of steering the array in a specific direction. The effect of steering in wavenumber space is straightforward. Consider the processor in Figure 2.21.⁵ The basis function input to the steering section is

$$f(t, \mathbf{p}) = e^{j\omega t} \mathbf{v}_k(\mathbf{k}). \quad (2.118)$$

We would like the output to be aligned when

$$\mathbf{k} = \mathbf{k}_T, \quad (2.119)$$

the “target” wavenumber. We refer to \mathbf{k}_T as the **steering direction** or **main response axis** in \mathbf{k} -space. We accomplish this with an $N \times N$ diagonal

⁵The convention in our figures is that the vector or matrix in a box pre-multiplies the input.

steering matrix,⁶

$$\mathbf{I}_s(\mathbf{k}_T) \triangleq \begin{bmatrix} e^{j\mathbf{k}_T^T \mathbf{p}_1} & 0 & \cdots & 0 \\ 0 & e^{j\mathbf{k}_T^T \mathbf{p}_2} & \cdots & 0 \\ 0 & \cdots & \ddots & 0 \\ 0 & \cdots & 0 & e^{j\mathbf{k}_T^T \mathbf{p}_N} \end{bmatrix}. \quad (2.120)$$

The resulting output is

$$f_s(t, \mathbf{p}) = e^{j\omega t} \mathbf{v}_{\mathbf{k}}(\mathbf{k} - \mathbf{k}_T), \quad (2.121)$$

and the overall frequency wavenumber response is

$$\Upsilon(\omega, \mathbf{k} | \mathbf{k}_T) = \Upsilon(\omega, \mathbf{k} - \mathbf{k}_T). \quad (2.122)$$

The array response function is simply displaced to be positioned about \mathbf{k}_T . This is one of the useful aspects of using wavenumber space in interpreting array response functions. If we consider the beam patterns in wavenumber space, we also get a simple displacement.

When we use uniform amplitude weighting, the two-step process in Figure 2.21 is unnecessary. We let

$$\mathbf{w} = \frac{1}{N} \mathbf{v}_{\mathbf{k}}(\mathbf{k}_T) \quad (2.123)$$

and

$$B_c(\mathbf{k} : \mathbf{k}_T) = \frac{1}{N} \mathbf{v}_{\mathbf{k}}^H(\mathbf{k}_T) \mathbf{v}_{\mathbf{k}}(\mathbf{k}). \quad (2.124)$$

We refer to $B_c(\mathbf{k} : \mathbf{k}_T)$ as the **conventional beam pattern**. We will find that this conventional beam pattern plays a fundamental role in many of the optimum processing schemes that we will develop in the sequel.

For a linear array, the conventional beam pattern can be written as

$$B_{\psi c}(\psi : \psi_T) = \frac{1}{N} \mathbf{v}_{\psi}^H(\psi_T) \mathbf{v}_{\psi}(\psi) \quad (2.125)$$

in ψ -space and

$$B_{uc}(u : u_T) = \frac{1}{N} \mathbf{v}_u^H(u_T) \mathbf{v}_u(u) \quad (2.126)$$

⁶Note that for the wideband case, we accomplish (2.120) with delays. Only in the narrowband case can the delays be replaced with phase shifts.

in u -space. For a uniform linear array,

$$B_\psi(\psi : \psi_T) = \frac{1}{N} \frac{\sin(N\frac{\psi - \psi_T}{2})}{\sin(\frac{\psi - \psi_T}{2})}. \quad (2.127)$$

The steering direction in ψ -space corresponds to an interelement phase shift of ψ_T . In u -space,

$$B_u(u : u_T) = \frac{1}{N} \frac{\sin[\frac{\pi N d}{\lambda}(u - u_T)]}{\sin[\frac{\pi d}{\lambda}(u - u_T)]}. \quad (2.128)$$

Thus if we look at the expressions in (2.127), or (2.128), they all correspond to shifts in the pattern, but its shape is not changed. This property of shifting without distortion is one of many advantages of working in ψ -space or u -space.

As we steer the array so that the main response axis is aimed at $\bar{\theta}_0$, where $\bar{\theta}_0$ is the angle measured from broadside, the beam pattern shifts so that the center peak is at $u_0 = \sin \bar{\theta}_0$. This shift causes the grating lobes to move.

In Figure 2.22, we show the effect of steering on the beam pattern. In Figure 2.22(a), we show the beam pattern for $d = 2\lambda/3$ and $\bar{\theta} = 30^\circ$. We see that, at this steering angle, the grating lobe is at the edge of the visible region.

In Figure 2.22(b), we show the beam pattern for $d = \lambda/2$ and $\bar{\theta} = 90^\circ$. The grating lobe is at the edge of the visible region.

In general, we require

$$\frac{d}{\lambda} \leq \frac{1}{1 + |\sin \bar{\theta}_{max}|}, \quad (2.129)$$

where $\bar{\theta}_{max}$ is the maximum angle to which the array will be required to steer, in order to avoid a grating lobe from moving into the visible region. This result follows from calculating the location of the first grating lobe as a function of d/λ with $\bar{\theta}_T = \bar{\theta}_{max}$. Thus, if the array is required to steer $-90^\circ \leq \bar{\theta} \leq 90^\circ$, we require

$$d \leq \frac{\lambda}{2}. \quad (2.130)$$

The behavior in ψ -space and u -space is useful. However, it is important to remember that the signals originate in a (θ, ϕ) space, and we need to understand the behavior in that space.

In θ -space (i.e., angle space),

$$B_{\theta c}(\theta : \theta_T) = \frac{1}{N} \frac{\sin[\frac{\pi N d}{\lambda} (\cos \theta - \cos \theta_T)]}{\sin[\frac{\pi d}{\lambda} (\cos \theta - \cos \theta_T)]}. \quad (2.131)$$

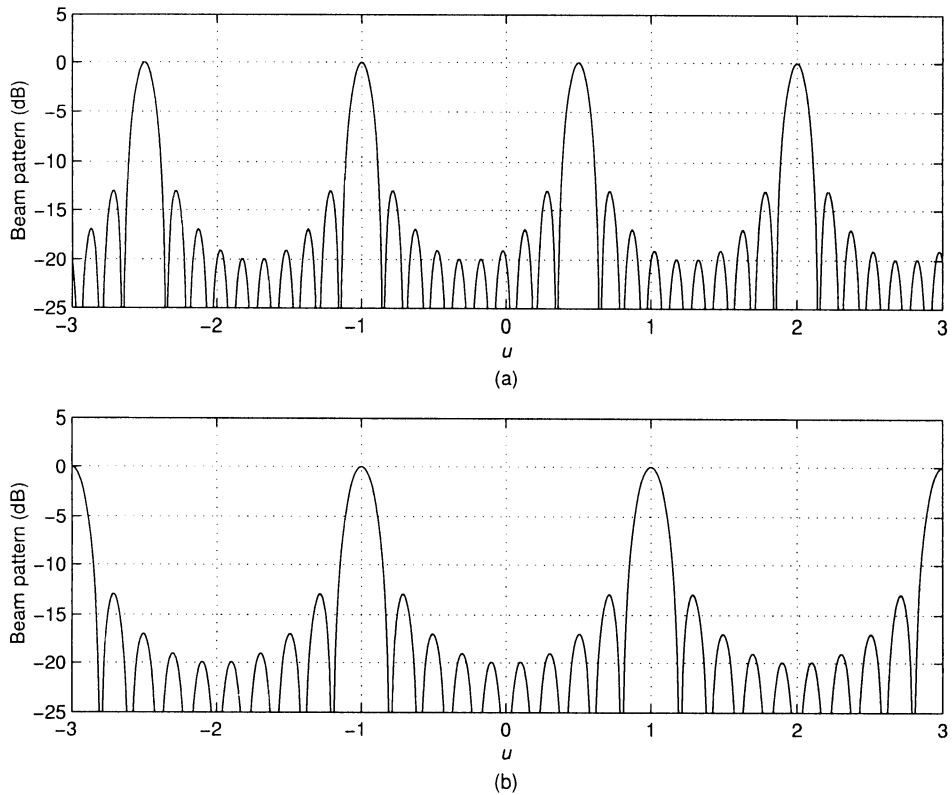


Figure 2.22 Effect of steering on the grating lobes: $N = 10$ (a) $d = 2\lambda/3, \bar{\theta} = 30^\circ$; (b) $d = \lambda/2, \bar{\theta} = 90^\circ$.

When we plot $B_{\theta c}(\theta : \theta_T)$ in θ -space, the shape of the pattern changes due to the $\cos\theta$ dependence. In Figure 2.23, we show the beam pattern for the case $\theta_T = 30^\circ$ and $d = \lambda/2$. Comparing this pattern with the pattern in Figure 2.17, we see that the beamwidth of the main lobe has increased.

To investigate the behavior of the HPBW in θ -space, we use (2.131) and (2.100). The right half-power point in u -space is

$$u_R = u_T + 0.450 \frac{\lambda}{Nd}, \quad (2.132)$$

and the left half-power point in u -space is

$$u_L = u_T - 0.450 \frac{\lambda}{Nd}, \quad (2.133)$$

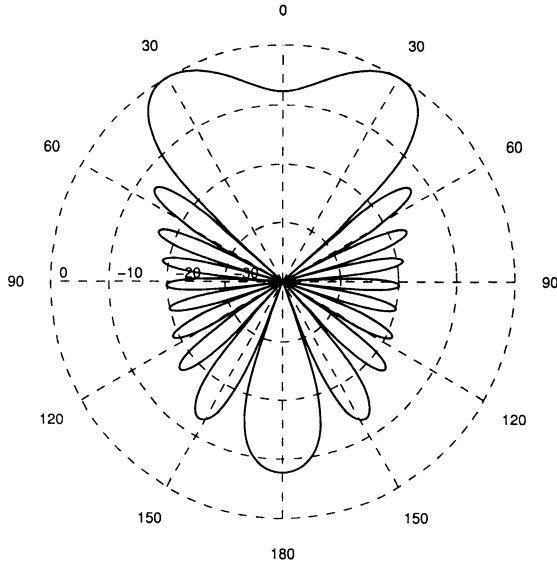


Figure 2.23 Beam pattern for 10-element uniform array ($d = \lambda/2$) scanned to 30° (60° from broadside).

or, in θ -space (θ_R corresponds to u_L and θ_L corresponds to u_R),

$$\cos \theta_R = \cos \theta_T - 0.450 \frac{\lambda}{Nd}, \quad (2.134)$$

$$\cos \theta_L = \cos \theta_T + 0.450 \frac{\lambda}{Nd}. \quad (2.135)$$

Thus, the half-power beamwidth in θ -space is

$$\begin{aligned} \theta_H = \theta_R - \theta_L &= \cos^{-1} \left[\cos \theta_T - 0.450 \frac{\lambda}{Nd} \right] + \\ &\quad \cos^{-1} \left[\cos \theta_T + 0.450 \frac{\lambda}{Nd} \right], \end{aligned} \quad (2.136)$$

for $0 \leq \theta \leq \pi$, $\theta_L, \theta_R \geq 0$. Except for the case when $\theta_T = 0$ or π (endfire), θ_L is defined to be the half-power point closest to $\theta = 0$. As the beam is steered from broadside ($\theta_T = \pi/2$) toward the positive z -axis (endfire, $\theta_T = 0$), the beam broadens. At some point, θ_L as given by (2.135) equals 0. Beyond that point there is no half-power point on that side of the beam. Elliott [Ell81] refers to this point as the scan limit.

The beamwidths given by (2.136) and (2.138) were plotted by Elliott [Ell81] and are shown in Figure 2.24.

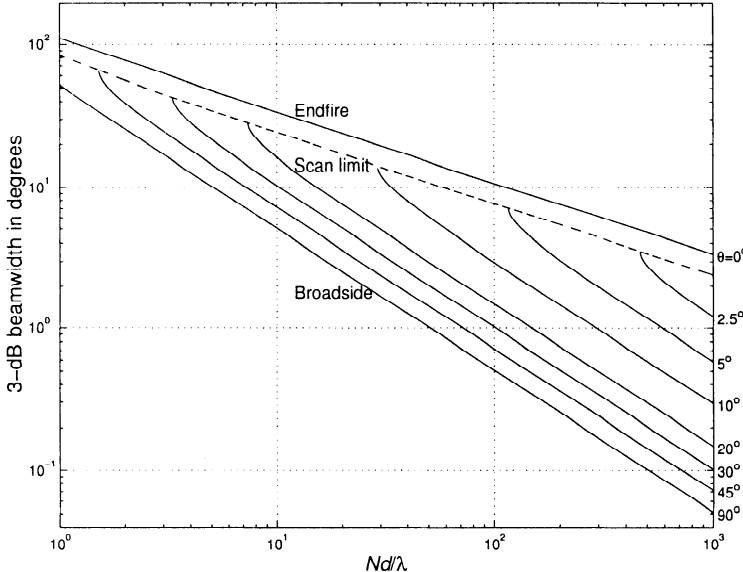


Figure 2.24 HPBW versus steering angle: standard linear array with uniform weighting.

When the beam is steered in the vicinity of broadside ($\bar{\theta}_T$ is small) and $Nd \gg \lambda$, θ_H will be small and we use a small angle expansion to obtain

$$\theta_H \simeq 0.891 \frac{\lambda}{Nd} \csc \bar{\theta}_T. \quad (2.137)$$

The behavior in (2.137) is apparent from Figure 2.25. The effective array length is reduced by $\cos \bar{\theta}_T$.

For $Nd \geq 5\lambda$, the result in (2.137) is in error by less than 0.2% near broadside and by less than 4% at the scan limit.

When $\theta_T = 0$ or π , the maximum response axis is pointed along the array axis and is referred to as an **endfire array**. The beam pattern for a standard 10-element endfire array is shown in Figure 2.26. In this case,

$$\theta_H = 2 \cos^{-1} \left[1 - 0.450 \frac{\lambda}{Nd} \right], \quad \theta_T = 0 \text{ or } \pi. \quad (2.138)$$

We can rewrite (2.138) as

$$1 - \cos \left(\frac{\theta_H}{2} \right) = 0.450 \frac{\lambda}{Nd} \quad (2.139)$$

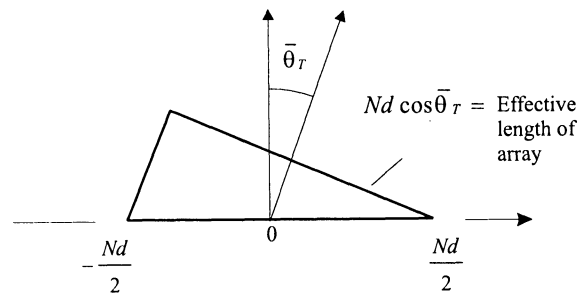


Figure 2.25 Effective array length reduced by $\cos \bar{\theta}_T$.

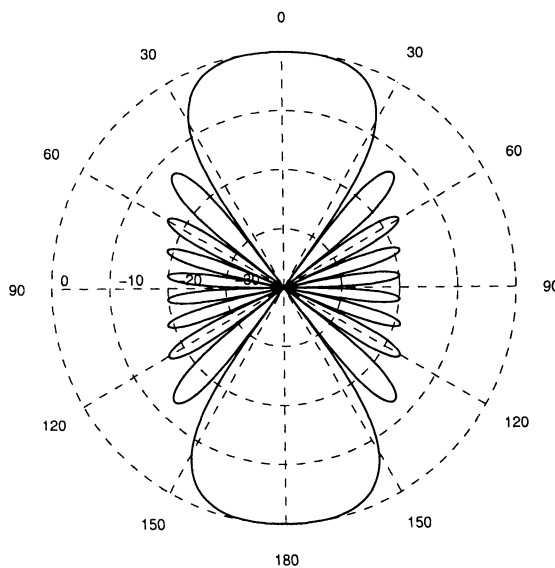


Figure 2.26 Beam pattern of a standard 10-element linear array with uniform amplitude weighting at endfire.

or

$$\sin\left(\frac{\theta_H}{4}\right) = \sqrt{\frac{0.450}{2} \cdot \frac{\lambda}{Nd}}. \quad (2.140)$$

For $Nd \gg \lambda$, θ_H is small and (2.140) becomes

$$\theta_H = 2\sqrt{0.890 \frac{\lambda}{Nd}}, \quad (2.141)$$

For $Nd \geq 5\lambda$, (2.141) is in error by less than 1%.

Similarly, the first null in the pattern is at

$$\theta_{null} = \sqrt{2 \frac{\lambda}{Nd}}. \quad (2.142)$$

Thus, the resolution of a linear array at endfire varies as the reciprocal of the square root of Nd/λ as contrasted to the linear dependence in the broadside case.

One can decrease the beamwidth of an endfire array by using a procedure proposed by Hansen and Woodyard [HW38]. This technique is described in Section 6.3.4 of [Bal82] and Section 4.7 of [Kra88]. We summarize the procedure in Problem 2.5.4.

2.6 Array Performance Measures

There are a number of performance measures by which one assesses the capabilities of an array. Each of the various measures attempts to quantify an important aspect of either the response of an array to the signal environment or of the sensitivity to an array design. We have already noted both the distance to the first nulls as a measure of the beamwidth or resolution of the frequency wavenumber response and the cardinal sidelobe levels of a uniformly weighted linear array. In this section we discuss three of the commonly used array performance measures:

- (i) Directivity
- (ii) Array gain versus spatially white noise (A_w)
- (iii) Sensitivity and the tolerance factor

2.6.1 Directivity

A common measure of performance of an array or aperture is the **directivity**. We will define it for the general case and then specialize it to a linear array.

We define the **power pattern**, $P(\theta, \phi)$, to be the squared magnitude of the beam pattern $B(\omega : \theta, \phi)$

$$P(\theta, \phi) = |B(\omega : \theta, \phi)|^2, \quad (2.143)$$

where the frequency dependence of $P(\theta, \phi)$ is suppressed in the notation. Then the directivity D is defined as

$$D = \frac{P(\theta_T, \phi_T)}{\frac{1}{4\pi} \int_0^\pi d\theta \int_0^{2\pi} d\phi \sin \theta \cdot P(\theta, \phi)}, \quad (2.144)$$

where (θ_T, ϕ_T) is the steering direction or main response axis (MRA).

In a transmitting array or aperture, D represents the maximum radiation intensity (power per unit solid angle) divided by the average radiation intensity (averaged over the sphere).

In a receiving antenna, we find in Chapter 5 that the denominator represents the noise power at the array (or aperture) output due to isotropic noise (noise distributed uniformly over a sphere). The numerator will represent the power due to a signal arriving from (θ_T, ϕ_T) . Thus, D can be interpreted as the array gain against isotropic noise.

If we assume that the weights are normalized so that $P_n(\theta_T, \phi_T) = 1$, then (2.144) can be written as

$$D = \left\{ \frac{1}{4\pi} \int_0^\pi d\theta \int_0^{2\pi} d\phi \sin \theta \cdot P(\theta, \phi) \right\}^{-1}. \quad (2.145)$$

For a linear array

$$B(\theta, \phi) = B(\theta), \quad (2.146)$$

so (2.145) becomes

$$D = \left\{ \frac{1}{2} \int_0^\pi |B(\theta)|^2 \sin \theta d\theta \right\}^{-1}. \quad (2.147)$$

This can be expressed in u -space as

$$D = \left\{ \frac{1}{2} \int_{-1}^1 |B_u(u)|^2 du \right\}^{-1}. \quad (2.148)$$

In general, this expression must be evaluated numerically.

Using (2.70), the expression in (2.148) can be written in terms of the array weights as

$$D = \left\{ \frac{1}{2} \int_{-1}^1 \sum_{n=0}^{N-1} w_n^* e^{jn(\frac{2\pi d}{\lambda})(u-u_T)} \sum_{m=0}^{N-1} w_m e^{-jm(\frac{2\pi d}{\lambda})(u-u_T)} du \right\}^{-1}. \quad (2.149)$$

where u_T is the steering direction in u -space. Rearranging terms and performing the integration gives

$$D = \left\{ \sum_{n=0}^{N-1} \sum_{m=0}^{N-1} w_m w_n^* e^{j(\frac{2\pi d}{\lambda})(m-n)u_T} \text{sinc}\left(\frac{2\pi d}{\lambda}(n-m)\right) \right\}^{-1}. \quad (2.150)$$

We define several matrices to obtain a compact expression. The n, m element of the **sinc** matrix is

$$[\text{sinc}]_{nm} \triangleq \text{sinc}\left(\frac{2\pi d}{\lambda}(n-m)\right). \quad (2.151)$$

The steering matrix in u -space is (2.120)

$$\mathbf{I}_{su} = \text{diag}(1, e^{j\frac{2\pi d}{\lambda}u_T}, e^{j\frac{2\pi d}{\lambda}2u_T}, \dots, e^{j\frac{2\pi d}{\lambda}(N-1)u_T}). \quad (2.152)$$

Then,

$$D = \mathbf{I}_{su} \mathbf{w}^H [\text{sinc}] \mathbf{w} \mathbf{I}_{su}^H. \quad (2.153)$$

Normally, we include the steering in the weight vector,⁷

$$\mathbf{w}_s = \mathbf{w} \mathbf{I}_{su}^H. \quad (2.154)$$

Then

$$D = \mathbf{w}_s^H [\text{sinc}] \mathbf{w}_s. \quad (2.155)$$

The standard linear array is a special case of interest. If $d = \lambda/2$, (2.150) reduces to

$$D = \left\{ \sum_{n=0}^{N-1} \sum_{m=0}^{N-1} w_m w_n^* e^{j\pi(m-n)u_T} \text{sinc}(\pi(n-m)) \right\}^{-1}. \quad (2.156)$$

The sinc function equals one when $m = n$ and zero when $m \neq n$, so (2.156) reduces to

$$D = \left\{ \sum_{n=0}^{N-1} |w_n|^2 \right\}^{-1} = (\mathbf{w}^H \mathbf{w})^{-2} = \left\{ \|\mathbf{w}\|^2 \right\}^{-1}, \quad (2.157)$$

⁷In most cases, the “ s ” subscript is dropped because we assume that \mathbf{w} includes steering.

where

$$\| \mathbf{w} \| = (\mathbf{w}^H \mathbf{w})^{\frac{1}{2}}, \quad (2.158)$$

is the 2-norm of the vector \mathbf{w} (A.36).

Thus, the directivity of a standard linear array is the reciprocal of the magnitude squared of the weight vector. The directivity does not depend on the steering direction. As the steering direction moves away from array broadside, the beam broadens but the circumference in the ϕ integration decreases.

For $d \neq \lambda/2$, we use the expression in (2.150) and the directivity will depend on the steering direction.

For a uniformly weighted standard linear array, $w_n = 1/N$, so

$$\sum_{n=0}^{N-1} |w_n|^2 = \frac{1}{N}, \quad (2.159)$$

so that

$$D = N. \quad (2.160)$$

Uniform weighting maximizes the directivity of the standard linear array. To show this, we constrain

$$\sum_{n=0}^{N-1} w_n = 1, \quad (2.161)$$

which guarantees that the beam pattern equals one for $u_T = 0$, and maximize $\sum_{n=0}^{N-1} |w_n|^2$. To perform the maximization, we write

$$F = \sum_{n=0}^{N-1} |w_n|^2 + \lambda \left(\sum_{n=0}^{N-1} w_n - 1 \right), \quad (2.162)$$

where λ is a Lagrange multiplier.⁸ Differentiating with respect to w_n and setting the result to zero gives

$$w_n^* = -\lambda \quad (2.163)$$

or

$$w_n = -\lambda^*. \quad (2.164)$$

Substituting (2.164) into (2.161) gives $\lambda^* = -1/N$, so

$$w_n = \frac{1}{N}, \quad (2.165)$$

⁸See Appendix A (Section A.7.4) for a discussion of complex gradients and the differentiation of a non-analytic function.

which is the desired result.

In Chapter 3, we discuss non-uniform weightings. The directivity always decreases. It is a function of the length of array measured in half wavelengths plus a term due to the non-uniform weighting.

The directivity of a standard uniformly weighted linear array can be related to the HPBW or the beamwidth between the first nulls. From Table 2.3, we have

$$D = \frac{4}{BW_{NN}}, \quad (2.166)$$

where the BW_{NN} is expressed in u -space. Note that (2.166) applies to a uniformly weighted array. For other weightings (2.166) may not hold.

Frequently, we express the directivity in dB and refer to it as the **directivity index**,

$$DI = 10 \log_{10} D. \quad (2.167)$$

We can write the DI as

$$DI = 10 \log_{10} N + 10 \log_{10}(g(\mathbf{w})). \quad (2.168)$$

The second term is a function of the weights. For any non-uniform weighting ($w_n \neq N^{-1}$), the DI will be reduced.

2.6.2 Array Gain vs. Spatially White Noise (A_w)

One of the purposes of an array is to improve the **signal-to-noise ratio (SNR)** by adding signals coherently and noise incoherently. The improvement is measured by the **array gain**. It is an important measure of array performance that we discuss extensively in later chapters. The general definition must be deferred until we introduce the spectral covariance matrix, which describes the statistical concepts for describing the spatial properties of the noise processes; however, we can formulate a restricted definition here.

We assume that the input at each sensor consists of a plane wave arriving along the main response axis plus a noise process that is uncorrelated among the sensors (spatially white noise). Thus,

$$x_n(t) = f(t - \tau_n) + n_n(t), \quad n = 0, \dots, N - 1. \quad (2.169)$$

At each sensor, the signal spectrum-to-noise spectrum ratio at frequency ω is

$$SNR_{in}(\omega) \triangleq \frac{S_f(\omega)}{S_n(\omega)}, \quad (2.170)$$

where the subscript “*in*” denotes input and the noise spectrum at each sensor is assumed to be identical.

In order to find the output due to the signal and noise, we need an expression for the output spectrum in terms of the beamformer weights and the input spectral matrix. From (2.8),

$$y(t) = \int_{-\infty}^{\infty} \mathbf{h}^T(\tau) \mathbf{x}(t - \tau) d\tau. \quad (2.171)$$

We assume that $\mathbf{x}(t)$ is zero-mean and wide-sense stationary. The correlation function of the output $y(t)$ is

$$R_y(\tau) = E[y(t)y^*(t - \tau)]. \quad (2.172)$$

The spectrum of $y(t)$ is

$$S_y(\omega) = \int_{-\infty}^{\infty} e^{-j\omega\tau} R_y(\tau) d\tau. \quad (2.173)$$

Using (2.171) in (2.172) and the result in (2.173) gives

$$S_y(\omega) = \int_{-\infty}^{\infty} e^{-j\omega\tau} d\tau \int_{-\infty}^{\infty} \mathbf{h}^T(\alpha) d\alpha \int_{-\infty}^{\infty} E[\mathbf{x}(t - \alpha)\mathbf{x}^H(t - \tau - \beta)] \mathbf{h}^*(\beta) d\beta. \quad (2.174)$$

This can be rewritten as

$$S_y(\omega) = \int_{-\infty}^{\infty} d\alpha \mathbf{h}^T(\alpha) e^{-j\omega\alpha} \int_{-\infty}^{\infty} dz e^{-j\omega z} \mathbf{R}_{\mathbf{x}}(z) \int_{-\infty}^{\infty} d\beta e^{-j\omega\beta} \mathbf{h}^*(\beta), \quad (2.175)$$

which reduces to

$$S_y(\omega) = \mathbf{H}^T(\omega) \mathbf{S}_{\mathbf{x}}(\omega) \mathbf{H}^*(\omega). \quad (2.176)$$

Using (2.52) in (2.176) gives the desired results,

$$S_y(\omega) = \mathbf{w}^H \mathbf{S}_{\mathbf{x}}(\omega) \mathbf{w}, \quad (2.177)$$

for the narrowband beamformer.

To calculate the output due to the signal, we impose the constraint on \mathbf{w} that,

$$\mathbf{w}^H \mathbf{v}_k(k_s) = 1. \quad (2.178)$$

The constraint in (2.178) implies that any signal arriving along \mathbf{k}_s will pass through the beamformer undistorted. We refer to the constraint in (2.178) as a **distortionless constraint**. It is used frequently in subsequent discussions.

We can write the input signal spectrum as

$$\mathbf{S}_f(\omega) = \mathbf{v}_k(k_s) S_f(\omega) \mathbf{v}_k^H(k_s). \quad (2.179)$$

Using (2.179) in (2.176), the output signal spectrum is

$$\begin{aligned} S_{y_s}(\omega) &= \mathbf{w}^H \mathbf{v}_k(k_s) S_f(\omega) \mathbf{v}_k^H(k_s) \mathbf{w} \\ &= S_f(\omega). \end{aligned} \quad (2.180)$$

The spectral output due to noise is

$$S_{y_n}(\omega) = \mathbf{w}^H \mathbf{S}_n(\omega) \mathbf{w}, \quad (2.181)$$

where $\mathbf{S}_n(\omega)$ is the spectral matrix of the input noise process. For the special case of spatial white noise and identical noise spectra at each sensor,

$$\mathbf{S}_n(\omega) = S_n(\omega) \mathbf{I}, \quad (2.182)$$

and

$$S_{y_n}(\omega) = \|\mathbf{w}\|^2 S_n(\omega) = \sum_{n=0}^{N-1} |w_n|^2 S_n(\omega). \quad (2.183)$$

Thus,

$$SNR_o(\omega) = \frac{1}{\sum_{n=0}^{N-1} |w_n|^2} \frac{S_f(\omega)}{S_n(\omega)}, \quad (2.184)$$

where the subscript “o” denotes output.

The array gain A_w reflects the improvement in SNR obtained by using the array. It is defined to be the ratio of the SNR at the output of the array to the SNR at an input sensor. The subscript “w” denotes the spatially uncorrelated noise input. The noise temporal frequency spectrum is not necessarily flat. Using (2.170) and (2.184),

$$A_w = \frac{SNR_o(\omega)}{SNR_{in}(\omega)} = \frac{1}{\sum_{n=0}^{N-1} |w_n|^2}, \quad (2.185)$$

or

$$A_w = \left(\sum_{n=0}^{N-1} |w_n|^2 \right)^{-1} = \|\mathbf{w}\|^{-2}. \quad (2.186)$$

Three observations with respect to (2.186) are useful:

(i) The result is valid for an arbitrary array geometry, as long as

$$|\mathbf{w}^H \mathbf{v}_k(k_s)|^2 = 1. \quad (2.187)$$

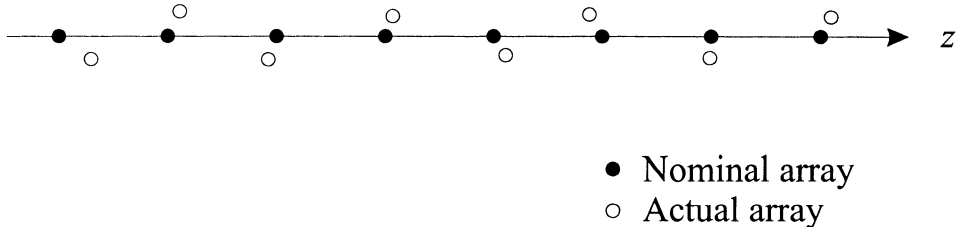


Figure 2.27 Array with position errors.

- (ii) For a standard linear array (spacing $d = \lambda/2$), the white noise array gain is identical to the array directivity (2.157). After we discuss isotropic noise fields in Chapter 5, the reason for this will be clear.
- (iii) For a uniform linear array with $d \neq \lambda/2$, D will not equal A_w . We will find the noise spectral matrix for an isotropic noise input is given by (2.151) so that D is the array gain A_{iso} for an isotropic noise input.

For a uniformly weighted array,

$$w_n = \frac{1}{N}, \quad n = 0, \dots, N - 1 \quad (2.188)$$

and $A_w = N$ (or $10 \log N$ in dB). A direct application of the Schwarz inequality shows that $A_w \leq N$. Therefore, if we are trying to maximize the array gain in the presence of spatially uncorrelated noise, a uniformly weighted array is optimum.

In Chapter 3, we will develop non-uniform weighting in order to improve sidelobe behavior. In these cases, we will be doing a trade-off between the loss in directivity and white noise array gain against improved sidelobe behavior.

2.6.3 Sensitivity and the Tolerance Factor

In later chapters, we analyze the sensitivity of optimum processors to gain and phase errors and imprecise positioning of the sensors. Here we summarize a typical result for the array shown in Figure 2.27. We design the processor so that, in the absence of array perturbations,

$$\mathbf{w}^H \cdot \mathbf{1} F(\omega) = F(\omega), \quad (2.189)$$

so that a signal from broadside passes through the array processing without distortion.

We consider the effect of filter perturbations and array location perturbations.

2.6.3.1 Filter perturbations

In this case we assume that the nominal matrix filter is \mathbf{w}^n . Denoting the i th component of \mathbf{w}^n as w_i^n , we can write the nominal weight as

$$(w_i^n)^* = g_i^n e^{-j\phi_i^n} \quad (2.190)$$

and the actual weight as

$$\begin{aligned} w_i^* &= g_i e^{-j\phi_i} \\ &= g_i^n (1 + \Delta g_i) e^{-j(\phi_i^n + \Delta\phi_i)}, \end{aligned} \quad (2.191)$$

where the Δg_i and $\Delta\phi_i$ are random variables.

2.6.3.2 Array location perturbations

In this case we assume that the nominal array locations are \mathbf{p}_i^n and that

$$\mathbf{p}_i = \mathbf{p}_i^n + \Delta \mathbf{p}_i. \quad (2.192)$$

Thus, we have the three variations from the nominal model:⁹

$$g_i = g_i^n (1 + \Delta g_i), \quad (2.193)$$

$$\phi_i = \phi_i^n + \Delta\phi_i, \quad (2.194)$$

$$\mathbf{p}_i = \mathbf{p}_i^n + \Delta \mathbf{p}_i. \quad (2.195)$$

The first two variations could result from changes in the gain and phase of the array sensors or from imperfect gain and phase in the processor filters. The last variation is caused by imperfect knowledge of the location of the array elements. We assume that the Δg_i ($i = 0, 1, \dots, N - 1$), the $\Delta\phi_i$ ($i = 0, 1, \dots, N - 1$), and the $\Delta p_{xi}, \Delta p_{yi}, \Delta p_{zi}$ ($i = 0, 1, \dots, N - 1$) are statistically independent, zero-mean, Gaussian random variables. We analyze the behavior of the beam pattern in the presence of these variations.

The nominal beam pattern is

$$\begin{aligned} B^{(n)}(\mathbf{k}) &= (\mathbf{w}^n)^H \mathbf{v}(\mathbf{k}) \\ &= \sum_{i=0}^{N-1} g_i^n \exp(j\phi_i^n - j\mathbf{k}^T \mathbf{p}_i^n). \end{aligned} \quad (2.196)$$

⁹This case is from Gilbert and Morgan [GM55]

The actual beam pattern is a random function. The expectation of its magnitude squared can be written as

$$\begin{aligned} \overline{|B(\mathbf{k})|^2} &\triangleq E\left\{ |B(\mathbf{k})|^2 \right\} \\ &= E\left\{ \sum_{i=0}^{N-1} \sum_{l=0}^{N-1} g_i \exp(j\phi_i - j\mathbf{k}^T \mathbf{p}_i) \right. \\ &\quad \left. \cdot g_l \exp(-j\phi_l + j\mathbf{k}^T \mathbf{p}_l) \right\} \end{aligned} \quad (2.197)$$

or

$$\begin{aligned} \overline{|B(\mathbf{k})|^2} &= \sum_{i=0}^{N-1} \sum_{l=0}^{N-1} E\left\{ g_i^n (1 + \Delta g_i) g_l^n (1 + \Delta g_l) \right. \\ &\quad \cdot \exp[j(\phi_i^n + \Delta\phi_i - \phi_l^n - \Delta\phi_l)] \\ &\quad \left. \cdot \exp[-j\mathbf{k}^T (\mathbf{p}_i^n + \Delta\mathbf{p}_i - \mathbf{p}_l^n - \Delta\mathbf{p}_l)] \right\}. \end{aligned} \quad (2.198)$$

Now define

$$\alpha_{il} = E\{(1 + \Delta g_i)(1 + \Delta g_l) \exp[j(\Delta\phi_i - \Delta\phi_l)]\} \quad (2.199)$$

and

$$\beta_{il}(\mathbf{k}) = E\left\{ \exp[-j\mathbf{k}^T (\Delta\mathbf{p}_i - \Delta\mathbf{p}_l)] \right\}. \quad (2.200)$$

Using the independent Gaussian random variable assumption,

$$\alpha_{il} = \begin{cases} \exp(-\sigma_\phi^2), & i \neq l \\ 1 + \sigma_g^2, & i = l \end{cases} \quad (2.201)$$

and

$$\beta_{il}(\mathbf{k}) = \begin{cases} \exp(-\sigma_p^2 |\mathbf{k}|^2) = \exp\left(-\left[\frac{2\pi\sigma_p}{\lambda}\right]^2\right) \triangleq \exp(-\sigma_\lambda^2), & i \neq l, \\ 1, & i = l, \end{cases} \quad (2.202)$$

where

$$\sigma_\lambda \triangleq \frac{2\pi\sigma_p}{\lambda}. \quad (2.203)$$

In the expression for $\beta_{il}(\mathbf{k})$, we have assumed that the variance of each component of $\Delta\mathbf{p}_i$ is equal to σ_p^2 . The term σ_λ^2 is the scaled variance measured in wavelengths. Then,

$$\begin{aligned} \overline{|B(\mathbf{k})|^2} &= \sum_{\substack{i=0 \\ i \neq l}}^{N-1} \sum_{l=0}^{N-1} g_i^n g_l^n \exp(j\phi_i^n - j\phi_l^n) \exp[-j\mathbf{k}^T (\mathbf{p}_i^n - \mathbf{p}_l^n)] \end{aligned}$$

$$\cdot \exp \left[- \left(\sigma_{\phi}^2 + \sigma_{\lambda}^2 \right) \right] + \sum_{i=0}^{N-1} \left(1 + \sigma_g^2 \right) (g_i^n)^2. \quad (2.204)$$

Adding $(g_i^n)^2 \exp[-(\sigma_{\phi}^2 + \sigma_{\lambda}^2)]$, $i = 0, 1, \dots, N-1$ in the first term and subtracting the appropriate quantity from the second term gives

$$\begin{aligned} \overline{|B(\mathbf{k})|^2} &= |B^{(n)}(\mathbf{k})|^2 \exp[-(\sigma_{\phi}^2 + \sigma_{\lambda}^2)] \\ &\quad + \sum_{i=0}^{N-1} (g_i^n)^2 \left\{ (1 + \sigma_g^2) - \exp \left[-(\sigma_{\phi}^2 + \sigma_{\lambda}^2) \right] \right\}, \end{aligned} \quad (2.205)$$

where σ_{ϕ}^2 , σ_{λ}^2 , and σ_g^2 denote the variance of the corresponding random variables.

The random variation has two effects. The first term attenuates the beam pattern uniformly in \mathbf{k} . This uniformity is due to our assumption that the variations are not dependent on \mathbf{k} . It means that the beam pattern has a statistical bias. The expected value of the pattern along the MRA is less than unity. The second term is more critical. Define

$$T_{se} = \sum_{i=0}^{N-1} |w_i^n|^2 = \sum_{i=0}^{N-1} (g_i^n)^2 \quad (2.206)$$

as the **sensitivity function**. Then the second term becomes

$$\overline{|B_2(\mathbf{k})|^2} = T_{se} \{ 1 + \sigma_g^2 - \exp[-(\sigma_{\phi}^2 + \sigma_{\lambda}^2)] \}, \quad (2.207)$$

which for small variances reduces to,

$$\overline{|B_2(\mathbf{k})|^2} = T_{se} \{ \sigma_g^2 + \sigma_{\phi}^2 + \sigma_{\lambda}^2 \}. \quad (2.208)$$

Note that T_{se} is the inverse of the array gain for white noise, (see (2.185))

$$T_{se} = [A_w]^{-1} = \| \mathbf{w} \|^2. \quad (2.209)$$

Thus as the white noise array gain increases, the sensitivity decreases. For an N -element array, the maximum white noise gain is N and corresponds to uniform weighting. Thus, any array with non-uniform weighting will be more sensitive to parameter variations than the uniformly weighted array. The effect of the second term is to raise the expected value in the sidelobe region uniformly. This constant value across \mathbf{k} -space can have a major impact. In many array designs, we would like to put a perfect null ($|B(\mathbf{k})|^2 = 0$) in the direction of an interfering signal. We look at techniques for doing this in

Section 3.7. The implication of the term in (2.208) or (2.207) is that, if any of the variances (σ_g^2 , σ_ϕ^2 , σ_λ^2) are non-zero, then we can not obtain a perfect null.

The level of the floor in the expected value of the power pattern will depend on the sensitivity function, T_{se} , and the variance of the perturbations. The effect is to limit the depth of the nulls in the pattern.¹⁰

As an example, suppose

$$\sigma_T^2 \triangleq (\sigma_g^2 + \sigma_\phi^2 + \sigma_\lambda^2) = 0.01. \quad (2.210)$$

Then, A_w must be greater than or equal to 100 in order to get -40 -dB nulls in the pattern. This requires that a uniformly weighted array must contain at least 100 elements. An array with non-uniform weighting would require even more elements.

Later in the text, when we design optimum arrays, we often impose a **sensitivity constraint**,

$$T_{se} = \| \mathbf{w} \|^2 \leq T_o, \quad (2.211)$$

where T_o is a design constant to make the performance more robust to perturbations. The constraint in (2.211) is often referred to as a **white noise gain constraint**,

$$A_w = (\| \mathbf{w} \|^2)^{-1} \geq T_o^{-1}. \quad (2.212)$$

In many of the design problems that we consider later, we find that the constraint in (2.211) plays an important role.

2.6.4 Summary

In this section, we have developed three important array performance measures. We observe that the norm of the weight vector \mathbf{w} has appeared in all three measures:

- (i) For a standard linear array, the directivity is

$$D = \| \mathbf{w} \|^2 \leq N.$$

- (ii) For any array geometry, the white noise array gain is

$$A_w = \| \mathbf{w} \|^2.$$

¹⁰In mathematical terms, a null in the beam pattern means $B(\mathbf{k}) = 0$. However, in practice, the actual pattern has some non-zero value. The ratio of this value to the value at $B(\mathbf{k}_T)$ is referred to as the **null depth**.

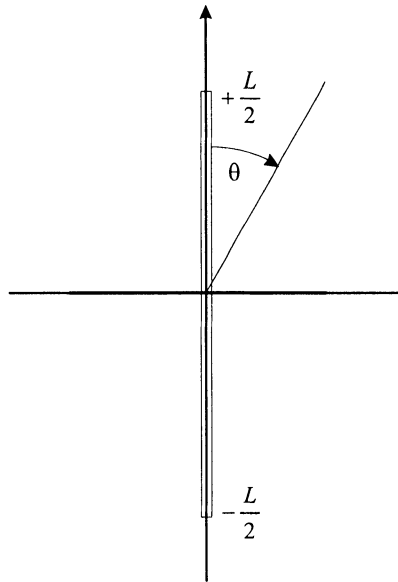


Figure 2.28 Linear aperture.

(iii) For any array geometry, the sensitivity function is

$$T_{se} = A_w^{-1} = \| \mathbf{w} \|^2.$$

Later we will see that $\| \mathbf{w} \|^2$ will play a central role in many of our discussions.

2.7 Linear Apertures

2.7.1 Frequency-wavenumber Response

Consider the linear aperture shown in Figure 2.28. We assume that it is steered to broadside and has an aperture weighting function $w_a^*(z)$, where “a” denotes “aperture.”

The frequency-wavenumber response function is given by

$$\Upsilon(\omega, k_z) = \int_{-L/2}^{L/2} dz w_a^*(z) e^{-jk_z z}. \quad (2.213)$$

The exponential term, $\exp(-jk_z z)$, is the **array manifold function** and is analogous to the array manifold vector in an array. Observing that

$$w_a^*(z) = 0, \quad |z| > \frac{L}{2}, \quad (2.214)$$

we have

$$\boxed{\Upsilon(\omega, k_z) = \int_{-\infty}^{\infty} w_a^*(z) e^{-jk_z z} dz,} \quad (2.215)$$

which is familiar as the Fourier transform. The inverse transform is

$$\boxed{w_a^*(z) = \frac{1}{2\pi} \int_{-\infty}^{\infty} \Upsilon(\omega, k_z) e^{jk_z z} dk_z.} \quad (2.216)$$

We see that the aperture weighting function and the frequency-wavenumber response are a Fourier transform pair in the $z - k_z$ variables. Thus all the Fourier transform properties can be applied to the aperture problem. For a linear aperture with uniform weighting,

$$\begin{aligned} \Upsilon(\omega, k_z) &= \int_{-L/2}^{L/2} \frac{1}{L} e^{-jk_z z} dz \\ &= \frac{e^{j\frac{L}{2}k_z} - e^{-j\frac{L}{2}k_z}}{2j(k_z \frac{L}{2})} \\ &= \frac{\sin(\frac{L}{2}k_z)}{\frac{L}{2}k_z}, \quad -\infty < k_z < \infty \end{aligned} \quad (2.217)$$

or¹¹

$$\Upsilon(\omega, k_z) = \text{sinc}\left(\frac{L}{2}k_z\right), \quad -\infty < k_z < \infty, \quad (2.218)$$

and, since $k_z = -(2\pi/\lambda)u$,

$$B_u(u) = \text{sinc}\left(\frac{\pi L}{\lambda} u\right), \quad -1 \leq u \leq 1. \quad (2.219)$$

The function is plotted in Figure 2.29.

It is useful to compare the result in (2.219) with the array result in (2.96). To find the equivalent length of aperture corresponding to an array of N elements, we equate the arguments of the sine functions in the numerators of (2.219) and (2.96),

$$\frac{\pi L}{\lambda} u = \frac{\pi N d}{\lambda} u. \quad (2.220)$$

This equality provides the same main lobe width and null spacing. Thus,

$$L = N d. \quad (2.221)$$

This relationship is shown in Figure 2.30. The equivalent length aperture extends $d/2$ beyond the actual array length in each direction.

¹¹We define $\text{sinc } x$ as $(\sin x)/x$. Some sources (e.g., MATLAB®) define $\text{sinc } x$ as $(\sin(\pi x))/(\pi x)$.

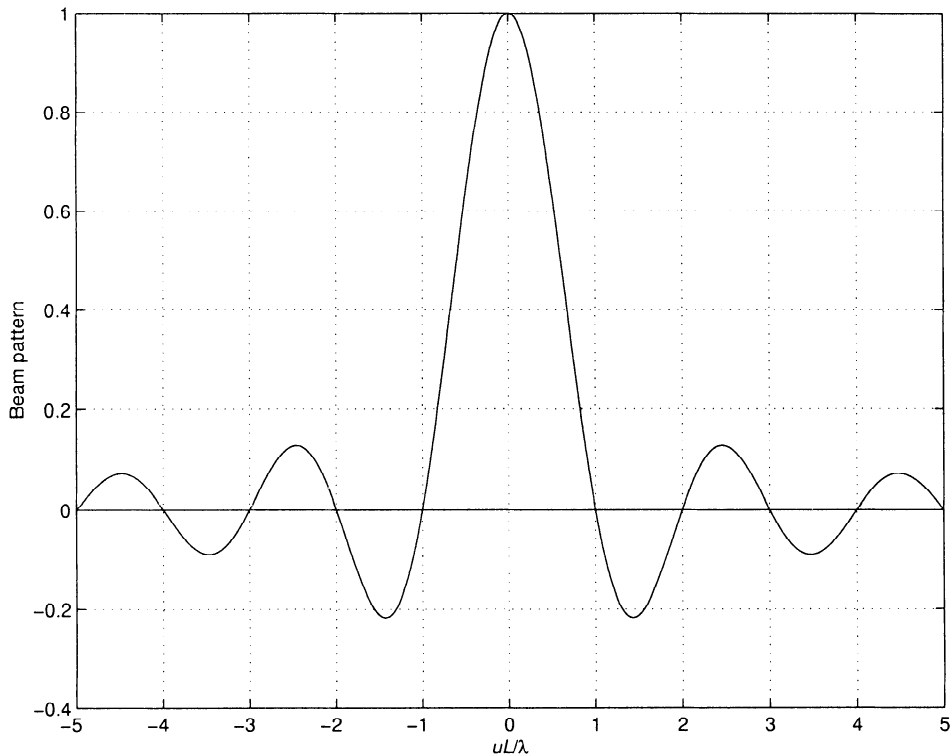


Figure 2.29 Beam pattern of uniformly weighted linear aperture.

One Fourier transform property of immediate use is the shifting property. The array in (2.213) is steered to broadside. To steer to k_{zT} , we have

$$\Upsilon(\omega, k_z : k_{zT}) = \Upsilon(\omega, k_z - k_{zT}). \quad (2.222)$$

Substituting into (2.216) gives

$$\begin{aligned} w_a^*(z : k_{zT}) &= \frac{1}{2\pi} \int_{-\infty}^{\infty} \Upsilon(\omega, k_z - k_{zT}) e^{jzk_z} dk_z \\ &= \frac{1}{2\pi} \int_{-\infty}^{\infty} \Upsilon(\omega, \Delta k) e^{jz(\Delta k + k_{zT})} d(\Delta k) \\ &= e^{jzk_{zT}} w_a^*(z). \end{aligned} \quad (2.223)$$

Thus, as we have seen with arrays, steering the beam in wavenumber space corresponds to a progressive phase shift in the weighting function.

In many cases, we want to start the analysis with the linear aperture and

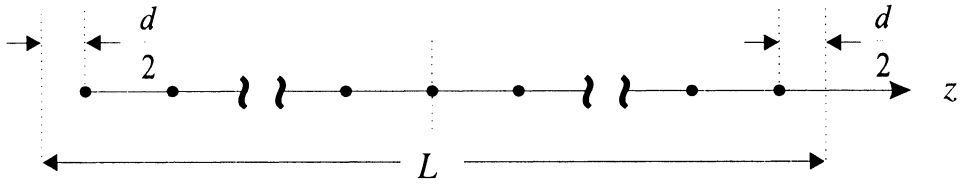


Figure 2.30 Equivalent apertures and arrays.

then implement its frequency wavenumber response by using an array. This leads us to the aperture sampling problem.

2.7.2 Aperture Sampling

Consider the continuous aperture shown in Figure 2.30. We want to replace it with the equivalent uniformly spaced array in Figure 2.30. The element spacing is d and we assume N is odd.

We can represent the array weighting function as a continuous aperture weighting function using a sum of impulse functions,

$$w_a^*(z) = \sum_{n=0}^{N-1} w_n^* \delta(z - (n - \frac{N-1}{2})d), \quad (2.224)$$

where $Nd = L$. Then, using (2.215),

$$\Upsilon(\omega, k_z) = \int_{-\infty}^{\infty} \sum_{n=0}^{N-1} w_n^* \delta(z - (n - \frac{N-1}{2})d) e^{-j k_z z} dz. \quad (2.225)$$

Integrating, we obtain

$$\Upsilon(\omega, k_z) = \sum_{n=0}^{N-1} w_n^* e^{-j(n - \frac{N-1}{2})k_z d}, \quad (2.226)$$

which is identical to (2.58).

If the continuous aperture weighting function is $w_a^*(z)$, then using a standard linear array ($d = \lambda/2$) with element weightings

$$w_n^* = w_a^*(z_n), \quad n = 0, 1, \dots, N-1, \quad (2.227)$$

will not, in general, produce an identical beam pattern. Usually, the sampled pattern will have very similar main-lobe behavior, but its sidelobe behavior will be different. We see examples of this behavior in Chapter 3.

If our goal is to duplicate the beam pattern of continuous aperture, we can use smaller interelement spacing.

2.8 Non-isotropic Element Patterns

Our discussion up to this point has assumed that each element had an isotropic response. In many cases, each element will have a beam pattern. In other cases, groups of sensors may be combined into a subarray with a beam pattern. The subarrays are treated as elements in the overall array. It is straightforward to incorporate these element beam patterns through pattern multiplication.

We assume each element is a linear aperture and has an identical weighting, denoted by $w_{ae}^*(z)$. These elements are configured into a linear array at location z_n , $n = 0, 1, \dots, N - 1$. Note that the spacing does not have to be uniform. The array weightings are w_n^* . The total weighting function is,

$$w_a^*(z) = \sum_{n=0}^{N-1} w_n^* \cdot w_{ae}^*(z - z_n). \quad (2.228)$$

The resulting frequency-wavenumber function is

$$\begin{aligned} \Upsilon(\omega, k_z) &= \int_{-\infty}^{\infty} \sum_{n=0}^{N-1} w_n^* \cdot w_{ae}^*(z - z_n) e^{-jk_z z} dz \\ &= \sum_{n=0}^{N-1} w_n^* e^{-jk_z z_n} \int_{-\infty}^{\infty} w_{ae}^*(z_1) e^{-jk_z z_1} dz_1. \end{aligned} \quad (2.229)$$

The first term is familiar as the beam pattern of the array with isotropic elements. It is now convenient to denote it as the **array factor**

$$AF(k_z) \triangleq \sum_{n=0}^{N-1} w_n^* \cdot e^{-jk_z z_n}, \quad (2.230)$$

which is analogous to the expression in (2.58).

The second term is the element frequency-wavenumber function. Thus,

$$\Upsilon(\omega, k_z) = AF(k_z) \Upsilon_e(\omega, k_z). \quad (2.231)$$

In terms of beam patterns

$$B_u(u) = AF(u) B_{ue}(u), \quad (2.232)$$

where

$$k_z = -\frac{2\pi}{\lambda} \cos \theta = -\frac{2\pi}{\lambda} u. \quad (2.233)$$



Figure 2.31 Array of colinear apertures.

Thus, the total beam pattern is the product of the array factor and the element beam pattern. This behavior is referred to as pattern multiplication.

The derivation for three dimensions follows easily:

$$\Upsilon(\omega, \mathbf{k}) = AF(\mathbf{k})\Upsilon_e(\omega, \mathbf{k}). \quad (2.234)$$

Three representative cases are shown in figures 2.31, 2.32, and 2.33.

In the first case, the element is colinear with the linear array axis, and the resulting pattern can be represented in k_z -space.

In the second case, the element is perpendicular, so that the resulting pattern must be represented in \mathbf{k} -space (see Problem 2.8.3).

In the third case, the array is a rectangular planar array. If we consider the sensors in the x -direction to be elements of a linear array along the z -axis and each column has identical weightings, then the total array factor is the product of the two array factors,

$$AF(\mathbf{k}) = AF_z(\mathbf{k}) \cdot AF_x(\mathbf{k}). \quad (2.235)$$

In addition to non-isotropic beam patterns, there are other sensor characteristics that should be considered in a particular physical problem. In some situations, there may be mutual coupling between the sensors. Several references (e.g., Balanis [Bal82], Yeh et al. [YLU89], Friedlander and Weiss

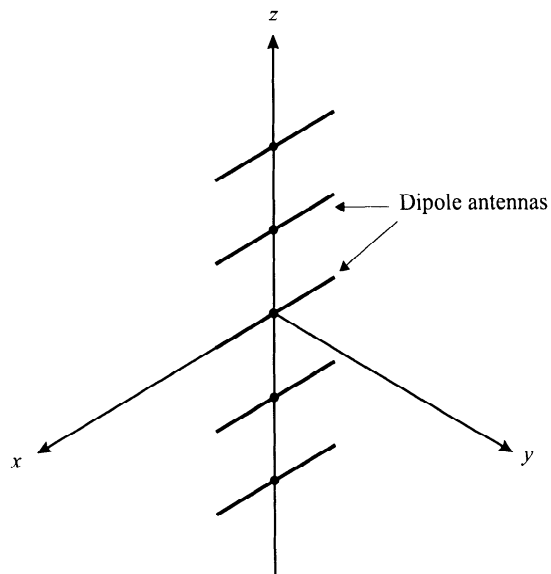


Figure 2.32 Array of dipoles.

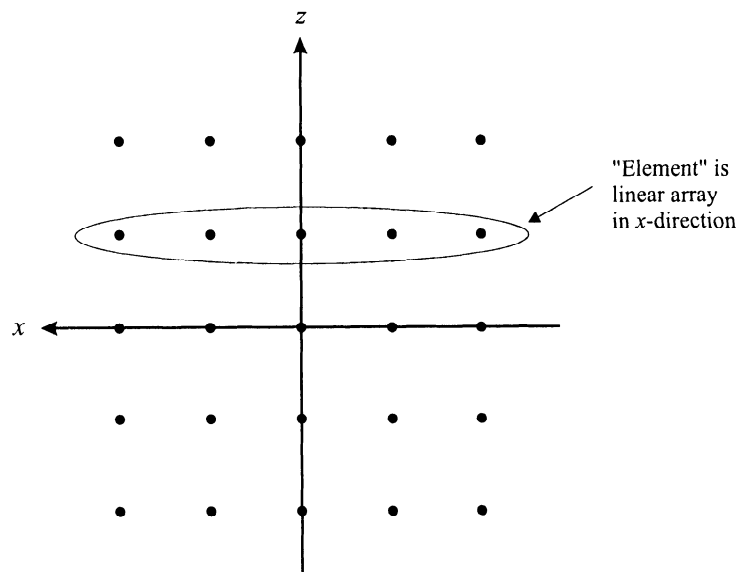


Figure 2.33 Planar array.

[FW91], and Svantesson [Sva99]). At several points in the text we will point out the effect of mutual coupling but will not pursue it in detail.

2.9 Summary

In this chapter, we have introduced many of the key concepts that will be used throughout the text.

In Section 2.2, we introduced the idea that the sensor array followed by a linear processor acts as spatial-temporal filter in (ω, \mathbf{k}) -space whose characteristics are described by a frequency-wavenumber function $\Upsilon(\omega, \mathbf{k})$, (2.37). In the visible region, the frequency-wavenumber function corresponds to the beam pattern, (2.38). The shape of these functions are determined by array geometry and the element weightings. The effect of array geometry is described by the array manifold vector, $\mathbf{v}_k(\mathbf{k})$, (2.28). For narrowband processors, the element weightings are complex gains, (2.49).

In Section 2.3, we considered a narrowband, uniform linear array and derived its array manifold vector, (2.73). We observed that the array manifold vector was conjugate symmetric, (2.74), (2.75). This symmetry will lead to computational simplifications in several situations.

In Section 2.4, we considered a uniformly weighted uniform linear array that often referred to as the conventional beamformer. The frequency-wavenumber function was given by (2.92), and the beam pattern was given by (2.95)–(2.97). We defined various beam pattern parameters; HPBW, BW_{NN} , SLL, and grating lobes. These parameters provide a good general description of the beam pattern.

In Section 2.5, we discussed array steering. Steering causes a translation of the beam pattern in k_z , ψ , or u -space, but causes pattern distortion in θ -space.

In Section 2.6, we introduced three important concepts: directivity, white noise array gain, and the sensitivity function. For a given array geometry, the directivity is maximized by a uniform weighting. In Chapter 3, we will study different array weightings and find that the design problem is to find a suitable trade-off between improving sidelobe behavior and the null placement and reducing the directivity. We found that the sensitivity function is the inverse of the white noise gain and equals the norm of the weight vector \mathbf{w} , (2.209).

In Section 2.7, we discussed linear apertures and found that the frequency-wavenumber function for a uniformly weighted linear aperture was a sinc function, (2.218), (2.219). We introduced aperture sampling in order to

approximate the aperture behavior with a uniform array.

In Section 2.8, we considered the case in which the sensor beam patterns are non-isotropic. We derived the pattern multiplication result.

This completes our discussion of uniformly weighted linear arrays. In Chapter 3 we discuss different weightings to improve the sidelobe performance of linear arrays.

2.10 Problems

The problems are divided corresponding to major sections in the chapter.

P2.3 Uniform Linear Arrays

Problem 2.3.1

Assume that N is even. Use the relationships

$$B_\psi(\psi) = 2\operatorname{Re} [\mathbf{w}_1^H \mathbf{v}_{\psi_1}(\psi)] \quad (2.236)$$

from (2.77) to derive the beam pattern of a uniformly weighted uniform linear array.

Problem 2.3.2

When N is odd, we can partition the array manifold vector of a uniform linear array into three parts,

$$\mathbf{v}_\psi(\psi) = \begin{bmatrix} \mathbf{v}_{\psi_1}(\psi) \\ 1 \\ \mathbf{J} \mathbf{v}_{\psi_1}^*(\psi) \end{bmatrix}. \quad (2.237)$$

Repeat Problem 2.3.1 for this case.

Problem 2.3.3

Show that, if \mathbf{w} is real and symmetric, then $B_\psi(\psi)$ for a uniform linear array is a real symmetric function. Consider both N even and N odd.

Problem 2.3.4

Assume that N is even. In some applications, we want to obtain an asymmetric beam pattern. Show that, if $\mathbf{v}_\psi(\psi)$ is conjugate symmetric and \mathbf{w} is real asymmetric, that is,

$$\mathbf{w} = \begin{bmatrix} \mathbf{w}_1 \\ -\mathbf{J} \mathbf{w}_1^* \end{bmatrix}, \quad (2.238)$$

where \mathbf{w}_1 is real, then $B_\psi(\psi)$ will be an imaginary function.

Problem 2.3.5

Repeat Problem 2.3.4 for N odd.

P2.4 Uniformly Weighted Linear Arrays

Problem 2.4.1

- (a) Construct a polar plot in dB of $B_\theta(\theta)$ for a standard 21-element linear array with uniform weighting for θ_T (the steering direction) equal to 0° , 15° , 30° , 60° , and 90° .
- (b) Find the HPBW for each of these θ_T .

Problem 2.4.2

Assume N is even and

$$w_n = \begin{cases} -\frac{1}{N} & n = 0, 1, \dots, \frac{N}{2} - 1, \\ \frac{1}{N} & n = \frac{N}{2}, \dots, N - 1. \end{cases} \quad (2.239)$$

- (a) Find the resulting beam pattern and plot the magnitude in dB and phase versus ψ for the case when $d = \lambda/2$.
- (b) Find the slope of the beam pattern at $\psi = 0$.

Problem 2.4.3

Consider a standard 10-element linear array with uniform weighting. Assume that the n th sensor fails. Plot the resulting beam pattern for several values of n .

Problem 2.4.4

Assume that each of the 10 sensors in Problem 2.4.3 are equally likely to fail with probability, $P_n(F) = \frac{1}{10}(1 - \alpha)$, where α is a reliability parameter whose value is in the range $[0, 1]$. Assume that, at most, one failure occurs.

- (a) Calculate the expected value of the beam pattern.
- (b) Plot the result for $\alpha = 0$ and $\alpha = 0.9$.
- (c) Does the expected value of the beam pattern provide a useful indication of the array behavior or do we have to consider the behavior on separate trials (as in Problem 2.4.3)?

Problem 2.4.5

Consider a standard 10-element linear array with uniform weighting. Assume that two sensors fail. Plot the resulting beam pattern for several values of n_1 and n_2 .

Problem 2.4.6

Consider the non-uniform 4-element linear array whose sensor separations are d , $3d$, $2d$ where $d = \lambda/2$. The sensor outputs are weighted uniformly.

- (a) Compute the beam pattern and BW_{NN} .
- (b) Compare the results in (a) with a uniform 7-element array with spacing where $d = \lambda/2$. Discuss the behavior of the main lobe and the sidelobes.

Problem 2.4.7

In order to find the exact HPBW, we must solve

$$|B_u(u)|^2 = 0.5,$$

where $B_u(u)$ is given by (2.96).

- (a) One approach to finding an approximate expression for the HPBW is to expand $|B_u(u)|^2$ in a second-order Taylor series around $u = 0$. Use the expression for $B_u(u)$ given in (2.126) to simplify the derivatives. Compare your result to the result in (2.98).
- (b) Use (2.96) to find the exact result as a function of N and compare the result with (2.98).

Problem 2.4.8

The second central moment of an array weighting function is defined as

$$\sigma_A^2 = \frac{\sum_{m=-\frac{N-1}{2}}^{\frac{N-1}{2}} m^2 w_m}{\sum_{m=-\frac{N-1}{2}}^{\frac{N-1}{2}} w_m}, \quad N \text{ odd}, \quad (2.240)$$

where the origin is at the center of gravity,

$$\sum_{m=-\frac{N-1}{2}}^{\frac{N-1}{2}} m w_m = 0. \quad (2.241)$$

The second-moment beamwidth is defined as

$$\Delta u_4 = \frac{\lambda}{4\sigma_A d}. \quad (2.242)$$

- (a) Find Δu_4 for a uniformly weighted linear array.
- (b) Compare to the HPBW.

Problem 2.4.9

Consider an 8-element linear array with $d = 5\lambda/8$ and uniform weighting. Plot $B_u(u)$. Compare the resulting beam pattern to the beam pattern of a standard 10-element linear array.

P2.5 Array Steering

Problem 2.5.1

The conventional beam pattern for an array is given by

$$B_\psi(\psi : \psi_T) = \mathbf{v}^H(\psi_T) \mathbf{v}(\psi). \quad (2.243)$$

- (a) Show that $B_\psi(\psi : \psi_T)$ is real if $\mathbf{v}(\psi)$ is conjugate symmetric.
- (b) Give two examples of conjugate symmetric array manifolds in addition to the uniform linear array.

Problem 2.5.2

Verify the result in (2.141) and plot the percentage error versus N for various λ .

Problem 2.5.3

In an ordinary endfire array, the beam pattern is obtained by letting

$$\psi = \frac{2\pi d}{\lambda} \cos \theta - \psi_T, \quad (2.244)$$

where

$$\psi_T = \frac{2\pi d}{\lambda}. \quad (2.245)$$

If $d = \lambda/2$, there are two identical endfire lobes, as shown in Figure 2.26. One way to reduce the back lobe is to reduce the wavelength. The visible region is $2(2\pi d/\lambda)$ wide in ψ -space. The first null in the back lobe is at $2\pi/N$ in ψ -space. Therefore if we reduce the visible region from the $d = \lambda/2$ value of 2π by $2\pi/N$, the back lobe should be significantly decreased. Thus,

$$2(2\pi d/\lambda) \leq 2\pi - \frac{2\pi}{N} \quad (2.246)$$

or

$$d \leq \frac{\lambda}{2}(1 - \frac{1}{N}). \quad (2.247)$$

- (a) Plot the beam pattern in u -space and θ -space for $N = 10$. In this case, $d = 0.45\lambda$ and $\psi_T = 0.9\pi$. Find the HPBW.

- (b) Consider the case where only part of the back lobe is moved out of the visible region. Let

$$d = \frac{\lambda}{2}(1 - \frac{1}{2N}). \quad (2.248)$$

Plot the beam pattern in u -space and θ -space for $N = 10$. Find the HPBW.

Problem 2.5.4 (Hansen-Woodyard)

In order to make the main beam narrower, Hansen and Woodyard [HW38] proposed moving part of the main lobe out of the visible region by increasing the interelement phase shift ψ_T ,

$$\psi_T = \left(\frac{2\pi d}{\lambda} + \frac{\pi}{N} \right). \quad (2.249)$$

However, the back lobe may move into the visible region unless d is decreased. To prevent the back lobe from becoming larger than the main lobe, we require $\psi_T < \pi$. Thus,

$$\frac{2\pi d}{\lambda} + \frac{\pi}{N} < \pi \quad (2.250)$$

or

$$d < \frac{\lambda}{2}(1 - \frac{1}{N}). \quad (2.251)$$

- (a) Consider a 10-element linear array. Let $d = 0.45\lambda$. Plot the beam pattern in u -space and θ -space. Find the HPBW.
(b) Repeat for $d = 0.3\lambda$, $d = 0.35\lambda$, and $d = 0.4\lambda$.
(c) Show that the nulls occur at

$$\theta_0 = 2\sin^{-1} \left[\pm \sqrt{\frac{\lambda}{4Nd}(2m-1)} \right]. \quad (2.252)$$

- (d) Show that, for long arrays,

$$\theta_0 \simeq \pm \sqrt{\frac{\lambda}{Nd}}(2m-1). \quad (2.253)$$

and the first zero occurs at

$$\theta_{01} \simeq \pm \sqrt{\frac{\lambda}{Nd}}. \quad (2.254)$$

Thus the null-null beamwidth is 0.707 times the width of an ordinary endfire array.

Problem 2.5.5

- (a) Consider a 10-element linear array pointed at endfire with $d = 3\lambda/8$. The progressive phase shift ψ_T is given by $\psi_T = 3\pi/4$. Plot $B_\theta(\theta)$.
- (b) Repeat part (a) with $\psi_T = \pi \left[\frac{3}{4} + \frac{1}{N} \right]$.

P2.6 Array Performance Measures

P2.6.1 Directivity

Problem 2.6.1

Consider a uniform N -element linear array with isotropic elements pointed at broadside with uniform weighting.

- (a) Plot the directivity versus d/λ over the range $0 \leq d/\lambda \leq 2.0$ for various N .
- (b) An approximate expression for D at broadside is

$$D = 2 \frac{Nd}{\lambda}, \quad 0 \leq d/\lambda \leq 1. \quad (2.255)$$

Superimpose this expression on the plot in part (a). Plot the error between the approximate expression and the exact value over the interval $0 \leq d/\lambda \leq 1$. Note that the expression is exact for $d = \lambda/2$ and that $D = N$.

Problem 2.6.2 (continuation)¹²

- (a) Calculate the directivity of the array in Problem 2.4.6.
- (b) Consider the general case pointed at broadside of a non-uniform linear array whose element locations are located on a grid whose points are separated by $d = \lambda/2$. Show that

$$D = \left(\sum_{n=0}^{N-1} |w_n|^2 \right)^{-1}, \quad (2.256)$$

where

$$\sum_{n=0}^{N-1} w_n = 1. \quad (2.257)$$

Therefore $D = N$ when the weighting is uniform.

Problem 2.6.3

Consider a standard 11-element linear array with triangular weighting,

$$w_n = c \left(1 - \frac{2|n - \frac{N-1}{2}|}{N} \right), \quad n = 0, 1, \dots, N-1, \quad (2.258)$$

¹²Continuation means that the problem assumes that either the previous problem or a specifically referenced problem has been read (or, in some cases, solved).

where

$$c = \left(\sum_{n=0}^{N-1} w_n \right)^{-1}. \quad (2.259)$$

- (a) Compute the directivity when the array is steered to broadside.
- (b) Generalize to an N -element array (N odd).

Problem 2.6.4

Consider a standard 5-element linear array pointed at broadside. We want to compare the following unnormalized weightings:

- (a) 1, 1, 1, 1, 1
- (b) 1, 2, 3, 2, 1
- (c) 1, 4, 6, 4, 1
- (d) 1, 1.61, 1.94, 1.61, 1
- (e) 1, 2.41, 3.14, 2.41, 1

Normalize the weightings. Plot the beam patterns in u -space and θ -space on separate plots. Compute D ; the HPBW in u -space and θ -space; the BW_{NN} in u -space and θ -space; and the height of the first sidelobe in dB. Discuss your results.

Problem 2.6.5

Repeat Problem 2.6.4 for an inverse triangular weighting,

3, 2, 1, 2, 3.

Discuss your result.

Problem 2.6.6

In order to find the directivity of a uniformly weighted linear array that is pointed at ψ_T , it is convenient to rewrite the beam pattern.

- (a) Show that

$$B_\psi(\psi) = \frac{1}{N} \left\{ 1 + 2 \sum_{m=1}^{\frac{N-1}{2}} \cos m\psi \right\}, \quad N \text{ odd}, \quad (2.260)$$

and

$$B_\psi(\psi) = \frac{1}{N} \left\{ 2 \sum_{m=0}^{\frac{N}{2}-1} \cos(m - \frac{N-1}{2})\psi \right\}, \quad N \text{ even}, \quad (2.261)$$

where

$$\psi = \frac{2\pi d}{\lambda} \cos \theta - \psi_T = \frac{2\pi d}{\lambda} \cos \theta - \frac{2\pi d}{\lambda} \cos \theta_T. \quad (2.262)$$

- (b) We then write

$$\left| \frac{\sin \frac{N\psi}{2}}{N \sin \frac{\psi}{2}} \right|^2 = \frac{1}{N} + \frac{2}{N^2} \sum_{m=1}^{N-1} (N-m) \cos m\psi. \quad (2.263)$$

Verify this expression for $N=2, 3, 4$, and 5.

(c) Show that

$$D = \left\{ \frac{1}{N} + \frac{2}{N^2} \sum_{m=1}^{N-1} \frac{(N-m)}{mk_0 d} \sin mk_0 d \cos m\psi_T \right\}^{-1}, \quad (2.264)$$

where ψ_T is the progressive phase factor. Thus,

$$\psi = k_0 d \cos \theta - \psi_T = \frac{2\pi d}{\lambda} \cos \theta - \psi_T. \quad (2.265)$$

The above result is for a set of N isotropic sources with an element spacing of d and an interelement phase shift ψ_T (e.g., p.142 of [ST81]).

- (d) Plot the directivity versus θ_T (in degrees) for a 5-element linear array. Consider $d = 0.3\lambda, 0.4\lambda, 0.5\lambda$, and 0.6λ .
- (e) Repeat part d for $N = 10$.

Problem 2.6.7

Show that the directivity of an ordinary endfire array ($\psi_T = 2\pi d/\lambda$) is approximately

$$D \simeq 4Nd/\lambda. \quad (2.266)$$

Problem 2.6.8

Show that the directivity of an Hansen-Woodyard endfire array is approximately

$$D \simeq 7.28 Nd/\lambda. \quad (2.267)$$

Problem 2.6.9

Consider a uniform 10-element linear array with uniform weighting pointed at endfire. Plot the directivity for the ordinary endfire array and the Hansen-Woodyard endfire array versus d/λ for the range $0.1 \leq d/\lambda \leq 0.6$.

When $D > N$, we refer to the array as superdirective. This problem shows a case of a practical superdirective array.

Problem 2.6.10

Consider the case of linear array whose element positions along the z -axis are z_n . The element phasings are linear with distance. Denote the phase of w_n as α_n . Then

$$\alpha_n = -\frac{2\pi}{\lambda} z_n \cos \theta_T. \quad (2.268)$$

- (a) Show that the beam pattern can be written as

$$B_\theta(\theta) = \frac{\sum_{n=0}^{N-1} |w_n| \exp(j(\frac{2\pi}{\lambda} z_n \cos \theta + \alpha_n))}{\sum_{n=0}^{N-1} |w_n|}. \quad (2.269)$$

- (b) Assume the weights are normalized so that

$$\sum_{n=0}^{N-1} |w_n| = 1, \quad (2.270)$$

then

$$\Omega_A \triangleq 2\pi \int_0^\pi |B_\theta(\theta)|^2 \sin \theta \, d\theta. \quad (2.271)$$

Use the result in part (a) to show that

$$\Omega_A = 2\pi \sum_{n=0}^{N-1} \sum_{m=0}^{N-1} |w_m| |w_n| e^{j(\alpha_n - \alpha_m)} \frac{\sin \left[\frac{2\pi}{\lambda} (z_n - z_m) \right]}{\frac{2\pi}{\lambda} (z_n - z_m)} \quad (2.272)$$

and

$$D = \frac{4\pi}{\Omega_A} = \left\{ \sum_{n=0}^{N-1} \sum_{m=0}^{N-1} |w_m| |w_n| e^{j(\alpha_n - \alpha_m)} \frac{\sin \left[\frac{2\pi}{\lambda} (z_n - z_m) \right]}{\frac{2\pi}{\lambda} (z_n - z_m)} \right\}^{-1} \quad (2.273)$$

P2.6.3 Sensitivity and the Tolerance Factor

Problem 2.6.11

Consider the special case of the perturbation model in Section 2.6.3 in which only the locations of the array elements are perturbed. Thus, (2.192) and the subsequent model applies. Assume that we have a standard N -element linear array along the z -axis and the only perturbations are in the z -direction.

- (a) Find the expected value of the beam pattern as a function of w_i^n and σ_λ^2 .
- (b) Plot the result for a 10-element array and uniform weighting for various σ_λ^2 .

Problem 2.6.12

Repeat Problem 2.6.11 for the case in which the only position perturbations are in the y -direction.

In part (b), plot the expected value of the beam pattern versus $u_z = \cos \theta$ for several values of ϕ .

Problem 2.6.13 (continuation Problem 2.6.4)

Calculate the sensitivity function for the five weightings in Problem 2.6.4.

Problem 2.6.14 (continuation)

- (a) Repeat Problem 2.6.11 for the case of phase-only errors. Therefore, (2.194) applies.
- (b) Compare your results with the results in Problem 2.6.11. Give an intuitive explanation of the comparison.

Problem 2.6.15

Consider a standard linear array designed for frequency f_c . We want to analyze the behavior for mismatched frequency. Assume the frequency of the incoming plane wave is f , where

$$f = \alpha f_c. \quad (2.274)$$

- (a) Plot the broadside beam pattern for $\alpha = 0.80, 0.90, 1.10, 1.20$.
- (b) Plot the directivity versus α over the range $0.5 < \alpha < 2.0$ for various scan directions: $\bar{\theta}_T = 0^\circ, 15^\circ, 30^\circ, 45^\circ$.

P2.7 Linear Apertures

Problem 2.7.1

Consider a linear aperture with $L = 5\lambda$. Assume that the weighting function is triangular.

- (a) Find an expression for the beam pattern and plot it.
- (b) How is the beam pattern in part (a) related to the beam pattern for uniform weighting?
- (c) Compare the result in part (a) to an equivalent linear array with $d = \lambda/4$ and $d = \lambda/2$.

Problem 2.7.2

The second central moment of the aperture weighting is defined as

$$\sigma_w^2 = \frac{\int_L z^2 w(z) dz}{\int_L w(z) dz}, \quad (2.275)$$

where the origin is at the center of gravity. The second-moment beamwidth is defined as

$$\Delta u_4 = \frac{\lambda}{4\sigma_w}. \quad (2.276)$$

Find Δu_4 for a rectangular weighting.

P2.8 Non-isotropic Element Patterns

Problem 2.8.1

The beam pattern for a short dipole ($L < \lambda$) aligned with the z -axis is

$$B_{DP}(\theta) = \sin \theta. \quad (2.277)$$

- (a) Find the beam pattern for the array in Figure 2.31.
- (b) Plot your result for $N = 10$.

Problem 2.8.2

The beam pattern for a short dipole ($L < \lambda$) aligned with the x -axis is

$$B_{DP}(\theta, \phi) = \frac{\cos \left[\left(\frac{\pi}{2} \right) \sin \theta \cos \phi \right]}{\sqrt{1 - \sin^2 \theta \cos^2 \phi}} \quad (2.278)$$

(e.g., pp.138–139 of [ST81]).

- (a) Find the beam pattern for standard linear array along the z -axis with uniform weighting.
- (b) Plot the beam pattern in the xz -plane and the yz -plane.

Problem 2.8.3 [ST81]

The directivity expression for a linear array with uniform weighting and non-isotropic elements is

$$D = \frac{1}{\frac{a_0}{N} + \frac{2}{N^2} \sum_{m=1}^{N-1} \frac{N-m}{mk_0d} (a_1 \sin mk_0d + a_2 \cos mk_0d) \cos m\psi_T} \quad (2.279)$$

where a_0 , a_1 , and a_2 are given in the table for various element patterns:

Element	$ B_e(\theta, \phi) ^2$	a_0	a_1	a_2
Isotropic	1	1	1	0
Collinear short dipoles	$\sin^2 \theta$	$\frac{2}{3}$	$\frac{2}{(mk_0d)^2}$	$\frac{-2}{mk_0d}$
Parallel to x -axis short dipoles	$1 - \sin^2 \theta \cos^2 \phi$	$\frac{2}{3}$	$1 - \frac{1}{(mk_0d)^2}$	$\frac{1}{mk_0d}$

- (a) Calculate the directivity for a 10-element linear array pointed at broadside with collinear short dipoles.
- (b) Repeat for parallel short dipoles.

Problem 2.8.4

Consider the planar array in Figure 2.32 and assume the elements are isotropic. Assume that $N_x = 10$, $N_z = 10$, $d_x = \lambda/2$. Find the beam pattern $B_{\theta, \phi}(\theta, \phi)$ when the array is pointed at broadside.

Plot the beam pattern versus $\cos \theta$ for several values of ϕ .

Problem 2.8.5

Consider a uniformly spaced planar array in the xy -plane with isotropic elements.

- (a) Find an expression for the beam pattern $B_{\theta, \phi}(\theta, \phi)$ when the array is pointed at broadside.
- (b) Plot the beam pattern for $N_x = N_y = 10$ and $d_x = d_y = \lambda/2$. Plot $B_{\theta, \phi}(\theta, \phi)$ versus $\cos \theta$ for various values of ϕ .
- (c) Repeat part (b) for the case in which the elements are short dipoles parallel to the z -axis.

Bibliography

- [Bal82] C. A. Balanis. *Antenna Theory: Analysis and Design*. Wiley, New York, 1982.
- [Ell81] R. S. Elliott. *Antenna Theory and Design*. Prentice-Hall, Englewood Cliffs, New Jersey, 1981.
- [FW91] B. Friedlander and A. J. Weiss. Direction finding in the presence of mutual coupling. *IEEE Trans. Antennas Propag.*, vol.AP-39, pp. 273–284, March 1991.
- [GM55] E.N. Gilbert and S.P. Morgan. Optimum design of directive antenna arrays subject to random variations. *Bell Syst. Tech. J.*, vol.34, pp. 637–663, May 1955.
- [HW38] W.W. Hansen and J.R. Woodyard. A new principle in directional antenna design. *Proc. IRE*, vol.26, pp. 333–345, March 1938.
- [Joh93] R. C. Johnson. *Antenna Engineering Handbook*. McGraw-Hill, New York, 3rd edition, 1993.
- [Kra88] J. D. Kraus. *Antennas*. McGraw-Hill, New York, 2nd edition, 1988.

- [Mil85] T. A. Milligan. *Modern Antenna Design*. McGraw-Hill, New York, 1985.
- [OS89] A. V. Oppenheim and R. W. Schafer. *Discrete-Time Signal Processing*. Prentice-Hall, Englewood Cliffs, New Jersey, 1989.
- [Sko80] M. I. Skolnik. *Introduction to Radar Systems*. McGraw-Hill, New York, 1980.
- [ST81] W. L. Stutzman and G. A. Thiele. *Antenna Theory and Design*. Wiley, New York, 1981.
- [Sva99] T. Svantesson. Modeling and estimation of mutual coupling in a uniform linear array of dipoles. *Proc. ICASSP*, vol.5, pp. 2961–2964, March 1999.
- [VT71] H. L. Van Trees. *Detection, Estimation, and Modulation Theory, Part III*. Wiley, New York, 1971.
- [VT01b] H. L. Van Trees. *Detection, Estimation, and Modulation Theory, Part III*. Wiley Interscience, New York, 2001.
- [Wee68] W. L. Weeks. *Antenna Engineering*. McGraw-Hill, New York, 1968.
- [YLU89] C. Yeh, M. Leou, and D. R. Ucci. Bearing estimations with mutual coupling present. *IEEE Trans. Antennas Propag.*, vol.AP-37, pp. 1332–1335, October 1989.
- [Zio95] L. J. Ziomek. *Fundamentals of Acoustic Field Theory and Space-Time Signal Processing*. CRC Press, Boca Raton, Florida, 1995.

Copyright of Optimum Array Processing is the property of John Wiley & Sons, Inc. 2002 and its content may not be copied or emailed to multiple sites or posted to a listserv without the copyright holder's express written permission. However, users may print, download, or email articles for individual use.